NASA-TM-112385

FLIGHT MEASUREMENTS OF BLADE-VORTEX INTERACTION NOISE INCLUDING COMPARISONS WITH FULL-SCALE WIND TUNNEL DATA

Gloria K. Yamauchi, David B. Signor, Michael E. Watts, and Francisco J. Hernandez

Aerospace Engineers
NASA Ames Research Center, Moffett Field, CA

and

Philip LeMasurier

Senior Technical Engineer
Sikorsky Aircraft Division, UTC
Trumbull, CT

PSB NASA
TN-71-TM
Canned
027224
30p.

Summary

Acoustic measurements of a Sikorsky S-76C helicopter in flight are presented. In addition, comparisons are made with acoustic measurements of a full-scale S-76 rotor tested in the 80- by 120-Foot Wind Tunnel at NASA Ames Research Center. The comparisons provide a preliminary determination of the validity of using the wind tunnel as an acoustic testing facility for full-scale rotor research and are the first direct comparison between in-flight and full-scale wind tunnel noise measurements. The investigation was designed to further the understanding of the blade vortex interaction noise generated by the S-76 rotor. The flight measurements were acquired using the NASA Ames YO-3A research aircraft fitted with acoustic instrumentation. Time-accurate separation distances between the S-76C and YO-3A were achieved using a portable laser rangefinder. Effects of tip-path-plane angle and advance ratio on the in-flight acoustics are presented for a limited number of conditions. Increasing tip-path-plane angle causes the BVI peaks to reach a maximum earlier in time; these observations are similar to those observed in two-bladed rotor flight test data and small-scale wind tunnel data. Flight and wind tunnel data are compared for three conditions. For the low and moderate advance ratio conditions presented, the BVI pulse widths and overall sound level of the flight and wind tunnel data are very similar. Comparisons between flight and wind tunnel data waveforms for the high advance ratio condition are poor.

Presented at the AHS 49th Annual Forum, St. Louis, Missouri, May 19-21, 1993. Copyright © 1993 by the American Helicopter Society, Inc. All rights reserved.

Notation

C_T	rotor thrust coefficient, thrust/$\pi R^2 \rho(\Omega R)^2$
dB	sound pressure level using corrected pressure referenced to 20 μPa
dB_{SL}	sound pressure level representing sum of energy in 1/3-octave bands with center frequencies from 100 Hz to 1000 Hz (using corrected pressure referenced to 20 μPa)
f	helicopter equivalent flat plate area, ft^2
I_s	helicopter shaft tilt offset (positive, shaft tilt rearward)
M_{tip}	hover tip Mach number, ΩR/(sound speed)
p	uncorrected pressure, Pa
p_o	static pressure of test condition, Pa
PSL	corrected pressure referenced to standard atmosphere sea level pressure, Pa
PSLo	standard atmosphere sea level pressure, Pa

R	rotor radius, ft
V_D	descent rate, ft/min (positive, descending)
V_{true}	true airspeed, kts
α_{tpp}	rotor tip-path-plane angle, deg (positive, rotor plane tilt rearward)
γ	glide slope angle, $\sin^{-1}(V_D/V_{true})$, deg (positive, descending)
μ	advance ratio, $V_{true}/\Omega R$
Ω	rotor rotational speed, rad/s
ρ	density, slug/ft^3
θ_f	helicopter attitude measured by gyroscope, deg (positive, nose up)

Introduction

Blade vortex interaction (BVI) noise has been extensively studied over the years because of the particularly annoying and detectable nature of the noise. The in-flight acoustic measurement method has played a key role in BVI research by providing data against which small-scale wind tunnel data and theoretical predictions have been compared.

The technique of acquiring acoustic measurements of helicopters in forward flight was developed over 15 years ago by Schmitz and Boxwell (Ref. 1), when noise measurements of a UH-1H were made using the OV-1C fixed wing aircraft as the "flying" acoustic platform. Vause et al. (Ref. 2) compared these measurements with 1/7-scale rotor data taken in the NASA Ames 7- by 10-Foot Wind Tunnel to investigate the scalability of high-speed impulsive noise. The acoustic waveforms were found to scale fairly well, establishing the validity of using small-scale data for the study of rotor high-speed impulsive noise, at least qualitatively. By 1980, the NASA Ames YO-3A research aircraft had been outfitted with acoustic instrumentation and subsequent in-flight measurements were made with this quiet aircraft. Boxwell and Schmitz (Ref. 3) conducted a flight test with the YO-3A and the two-bladed helicopters UH-1H and AH-1S. The investigation studied the differences in BVI noise of different main rotor blade sets. Schmitz et al. (Ref. 4) next compared the flight measurements of the AH-1S with 1/7-scale AH-1G/OLS rotor data acquired in the CEPRA-19 anechoic wind tunnel. The study showed that BVI was a scalable phenomenon for a two-bladed rotor provided the nondimensional parameters of thrust coefficient (C_T), advance ratio (μ), hover tip Mach number (M_{tip}) and rotor tip-path-plane angle (α_{tpp}) were matched between flight and wind tunnel tests. The same rotor was later tested in the aerodynamically cleaner and quieter Deutsch-Niederlaendischer Windkanal (DNW) open test section over a higher speed range. Splettstoesser et al. (Ref. 5) compared the high-speed impulsive noise from this small-scale test with the full-scale data of Ref. 3. A more in-depth study of BVI scalability using the same two data sets was next performed by Splettstoesser et al. (Ref. 6). BVI directivity and sensitivity to C_T, μ, M_{tip}, and α_{tpp} were investigated. The study showed that the BVI noise did not scale well at moderate to high advance ratios ($\mu > 0.22$).

BVI noise source location on the rotor disk and BVI noise directivity were studied in detail by Splettstoesser et al. (Ref. 7) and Martin et al. (Ref. 8), respectively. The subject rotor, a 40% dynamically scaled model of the BO-105 main rotor, was tested in the DNW. Traversing an array of microphones beneath the rotor plane generated a large test matrix. Blade-wake interactions and radiation patterns for a range of tip-path-plane angles and advance ratios were identified. As a result, Burley and Martin (Ref. 9) reported in detail the effects of tip-path-plane angle on BVI noise. Parametric (α_{tpp} and μ) effects on the movement of the strongest BVI noise radiation direction were determined by Martin et al. (Ref. 10) in a subsequent test in the DNW with the same rotor system. Other studies, for example, Marcolini et al. (Ref. 11), have been conducted using blade airloads data as input to analyses which then predict BVI noise.

A review of the literature reveals a deficiency in full-scale flight measurements of BVI noise. Measurements exist for two-bladed rotors only. In addition to the UH-1H and AH-1S flight tests discussed earlier, Cross and Watts (Ref. 12) acquired BVI noise measurements of the two-bladed AH-1G as part of the Tip Aerodynamics and Acoustic Test. With the exception of Ref. 12, this paper is the only published data acquired with the YO-3A in the past ten years and the only four-bladed rotor BVI noise in-flight data available in the open literature.

The In-Flight Rotorcraft Acoustics Program was recently established at NASA Ames Research Center. The program objective is to use the capabilities of the YO-3A to measure noise from helicopters whose main rotors were tested or will be tested in the National Full-Scale Aerodynamics Complex (NFAC) which includes the 40- by 80-Foot and 80- by 120-Foot Wind Tunnels. The program will help establish the validity of using the full-scale wind tunnels as acoustic testing facilities for full-scale rotor research. The attractive feature of this program is that no scaling of aerodynamic or acoustic phenomena is necessary since identical (geometric and dynamic) rotor systems can be tested in flight and in the wind tunnels.

This paper presents the results from an S-76 flight test, which is the first of a planned series of flight tests

with four-bladed rotors. This test was conducted jointly with Sikorsky Aircraft Division, United Technologies Corporation. Effects of tip-path-plane angle and advance ratio on BVI noise are presented and compared with trends observed in previous small-scale wind tunnel and two-bladed rotor flight tests. Limited comparisons are made with acoustic measurements acquired in the 80- by 120-Foot Wind Tunnel. A more complete comparison between flight and wind tunnel data is expected when the S-76 rotor system is tested in the 40- by 80-Foot Wind Tunnel.

Description of Test

S-76C Aircraft

The subject aircraft is a Sikorsky S-76C helicopter. Features of the helicopter are provided in Table 1. The S-76 rotor system is composed of four blades with coincident flap and lag articulation provided at the blade root by elastomeric bearings. Blade pitch motion is permitted by the same bearings. Figure 1 presents details of the rotor blade, which has a 22 ft radius with a 15.5 in nominal chord. Table 2 provides additional characteristics of the rotor system.

YO-3A Aircraft

The low tip speed of the nose-mounted propeller, a quiet belt-drive system, and a large muffler make the YO-3A a low-noise aircraft well suited for measuring in-flight helicopter noise. The YO-3A carries a pilot and flight engineer and is equipped with instrumentation for acoustic and flight condition data acquisition. Characteristics of the YO-3A are shown in Table 3. Further details about the YO-3A can be found in Cross (Ref. 13) and Cross and Watts (Ref. 14).

Flight Measurements

YO-3A Data Acquisition System. The YO-3A has condenser microphones mounted at each wingtip and at the top of the vertical tail. The microphones have diameters of 0.5 in and are fitted with bullet nose cones. A wing-mounted instrumentation boom provides indicated airspeed, altitude, outside air temperature, and angles of attack and sideslip. An analog tape recorder on board the YO-3A records the signals from the three microphones and the instrumentation boom. In addition, a time code and a once-per-revolution (1/rev) signal transmitted from the subject helicopter are recorded. The tape recorder voice channel is used to record flight condition parameters and pilots' comments for each flight test point. Once specified flight conditions are established, microphone gains are adjusted to insure maximum allowable signal response (2 V peak-to-peak); the gains are then hand-recorded. Signals are recorded continuously for 30 s at a tape speed of 30 in/s yielding a frequency range of DC to 20 kHz.

S-76C Data Acquisition System. A portable, eye-safe laser rangefinder was used from the passenger compartment of the S-76C to establish and maintain the desired separation distance from the YO-3A. A small section of the YO-3A starboard wing was used as a target for the laser. The distances were viewed using the heads-up display on the laser rangefinder and downloaded to a lap-top computer at a rate of 2 samples/s. The downloaded distance values were synchronized through the time code with the acoustic data recorded by the YO-3A data system. The capability of recording a time-accurate separation distance is a much-desired refinement to the previously used distance measuring technique. The helicopter attitude was measured by a gyro mounted on the floor of the S-76C and hand-recorded once during the 30 s of acoustic data recording.

Wind Tunnel Measurements

Acoustic measurements of a full-scale S-76 rotor were made in the 80- by 120-Foot Wind Tunnel at NASA Ames Research Center. Both the flight test and wind tunnel rotor blade systems were production S-76 systems, except for the one instrumented blade used in the wind tunnel. The rotor was mounted on the Rotor Test Apparatus (RTA). Figure 2 shows the S-76 rotor and RTA installed in the wind tunnel. The RTA includes a rotor balance which measures rotor lift, drag, and side-force. Measurements from the rotor balance were sent through a 100 Hz low-pass filter and acquired over a 30 s period, along with the tunnel conditions, at a rate of approximately 148 samples/s. The microphone selected for flight comparison was located two rotor diameters upstream of the rotor hub, nominally 25 deg down from the rotor plane at an azimuth of 150 deg. The microphone was the same type used in flight and was mounted on an acoustically-treated and faired stand hard-mounted to the wind tunnel floor (see Fig. 2). Once test conditions were established, the microphone signal and rotor 1/rev signal were recorded continuously for a minimum of 30 s at a tape speed of 30 in/s yielding a frequency range of DC to 20 kHz.

Flight Formation

The YO-3A tail-mounted microphone was selected as the primary microphone for wind tunnel comparison after

considering limited S-76C pilot visibility. Once the YO-3A pilot established the specified flight conditions, the S-76C was positioned such that the tail microphone was located in the desired position (two diameters upstream, nominally 25 deg down from the rotor plane, 150 deg rotor azimuth) relative to the hub. Figures 3(a) and 3(b) present a plan and side view of the formation, respectively. The angular alignment of the two aircraft was established visually by the S-76C pilot who aligned the top of the YO-3A tail with a target on the right wing of the YO-3A. The desired aircraft separation distance was established using the laser rangefinder. Figure 4 shows the "on condition" view from the passenger compartment of the S-76C. Figure 5 is a photograph of the formation viewed from the side.

Data Reduction Procedure

Acoustic Data

The Acoustic Laboratory Data Acquisition System (ALDAS), a Macintosh-based software package developed at NASA Ames, was used to reduce the majority of the data. Capabilities and features of ALDAS are described by Watts (Ref. 15). The acoustic signals were passed through an analog 2500 Hz low-pass filter and then digitized for 10 s or approximately 50 rotor revolutions. The mean value of the rotor rpm, determined from the recorded 1/rev signal, was used to calculate a digitization rate insuring nominally 2048 samples/rev (approximately 10000 samples/s). A calibration signal generated by a pistonphone and recorded before every flight was used to convert the digitized acoustic signal to pressure units. Next, a time history of one rotor revolution representing an average of 32 revolutions was constructed.

Averaging was performed in the time domain. A marker or feature existing in each revolution of data is needed to perform the averaging. The usual choice for the marker is the 1/rev spike recorded every revolution. Unfortunately, the rotor rpm during flight varies with gusts and slight adjustments to the helicopter controls. In addition, small changes in the separation distance between the S-76C and YO-3A causes time shifts in the recorded noise measurements. Therefore, using the 1/rev spike as an averaging marker will introduce smearing of the signal during averaging. A typical time history from the YO-3A tail mounted microphone includes four multi-peak events, representing the four blades, per rotor revolution. Each event consists of two to four spikes, where each spike is caused by a single BVI. These BVIs occur along the span of the blade at nearly the same time and so are referred to collectively as a single "event". In order to present an averaged signal while retaining the salient features of the four events, a feature evident in each of the four events and repeated throughout a minimum of 32 revolutions was chosen as the marker for averaging. For example, the marker could be a particular positive pressure peak. This marker may be different for different flight conditions. Figure 6 presents two events for one-half of a rotor revolution. For this example, the large positive peak is chosen as the marker. This procedure is not unlike the method used in Ref. 5 in averaging high-speed impulsive noise time histories. Because the time between events was also not constant, each of the four impulsive events was averaged separately over 32 revolutions. A composite time history of one rotor revolution was then constructed by piecing together the four averaged events. Because of the averaging technique used, zero time is not equivalent to zero degrees rotor azimuth.

Following the method of Ref. 5, the acoustic pressures were corrected to standard atmosphere, sea level pressure as shown below:

$$p_{SL}(t) = \frac{p(t)}{\left(\frac{p_o}{p_{SLo}}\right)} \qquad (1)$$

where p(t) represents the uncorrected acoustic pressure measured at altitude, p_o is the static pressure at altitude, and p_{SLo} is the standard atmosphere pressure at sea level. Spectra were generated from the corrected composite time history. Time histories are presented in terms of rotor revolution, achieved by normalizing time by the rotor speed. Finally, an overall sound level metric, dB_{SL}, was computed by summing the energy in the 1/3-octave bands with center frequencies from 100 Hz to 1000 Hz for each flight condition. This frequency range was considered to encompass the BVI frequencies.

The same procedures for digitizing and averaging were used for the wind tunnel acoustic data reduction for consistency. Since the 80- by 120-Foot Wind Tunnel is near sea level, the correction factor in Eq. (1) is close to unity. The overall sound level metric was also computed for the wind tunnel data.

Nonacoustic Data

Signals from the YO-3A instrumentation boom were digitized at 250 samples/s with no analog filtering over the same time period as the acoustic signals. Mean values were then extracted from the time histories and converted to engineering units using results from an extensive calibration prior to the flight test. The YO-3A rate of descent was determined from the slope of the altimeter signal time history. The helicopter weight at each flight condition was calculated assuming a constant fuel burn

rate and the time elapsed from engine start-up to the midpoint of the data record. Thrust coefficient, tip Mach number, and advance ratio were then computed. The following expressions show the two different methods used for computing tip-path-plane angle in flight:

$$\alpha_{tpp} = \gamma + \theta_f + I_s + a_{1s} \qquad (2)$$

$$\alpha_{tpp} = \gamma - \sin^{-1}\left(\frac{0.5\, f\, \mu^2}{C_T \pi R^2} \cos\gamma\right) \qquad (3)$$

Equation (2) uses the glide slope angle (γ), the helicopter attitude measured by the gyroscope (θ_f), and the shaft tilt offset angle (I_s=-5 deg). The S-76C was not instrumented to measure the longitudinal flapping angle, a_{1s}; therefore, a_{1s} is not included in the calculations of α_{tpp}. Equation (3), which is based on a simplified force model that excludes nonuniform inflow and pitch and roll moment effects, relies on the equivalent flat plate area (f=12.6 ft^2) of the helicopter. In the wind tunnel, the rotor tip-path-plane was assumed to be perpendicular to the rotor shaft since the first harmonic cyclic flapping was set nominally to zero. Therefore, the tip-path-plane angle is equivalent to the rotor shaft angle. No corrections for wall effects are applied. Mean tunnel conditions and rotor forces were computed by averaging over the 30 s data acquisition period.

Data Quality

Obtaining acoustic measurements in forward flight while maintaining a tight formation is a difficult procedure. The steadiness and consistency of the measurements depends on pilot skill and the atmospheric conditions. Acoustic measurements in a wind tunnel may be steadier, but are subject to contamination from reflections. The following discussion quantifies some of these sources of unsteadiness and contamination.

Flight Data

The establishment of the flight formation is initiated by the YO-3A pilot. As the lead aircraft, the YO-3A establishes a specified constant forward speed and descent rate. The S-76C pilot visually aligns the tip of the YO-3A tail with a target on the right wing to bring the helicopter into proper angular position. The accuracy of the angular alignment is estimated to be ±5 deg. While maintaining angular alignment, the S-76C pilot closes in on the YO-3A until the desired separation distance, as measured by the laser rangefinder, is achieved. The accuracy of the rangefinder is approximately ±2 ft. Once the two aircraft are "on condition", data are recorded for 30 s. The formation passes through the desired altitude approximately midway through the 30 s data record. As much as possible, the S-76C pilot refrains from adjusting controls during data acquisition. For the conditions presented in this paper, the sideslip angle was small (< 3 deg). By studying the recorded separation distances and listening to recorded comments made by both pilots, the steadiest 10 s period is extracted from the 30 s data record and digitized. Each flight condition was repeated at least twice. Flight points that were to be matched with wind tunnel data were repeated three times. This procedure prevented acquiring an extensive matrix of conditions, but did provide a measure of the repeatability of the flight data. For example, Fig. 7 shows repeated flight conditions. Although the magnitudes of some of the peaks in the events vary from Fig. 7(a) to 7(b), the details of the events repeat with reasonable consistency. A redundant method of computing the tip-path-plane angle was established by using Eqs. (2) and (3). Table 4 shows that the two equations produced values consistent with each other. Tip-path-plane angles shown in all figures were computed using Eq. (3).

The technique for averaging the acoustic time histories discussed earlier can be a source of error. In Ref. 5, this technique worked well in averaging high-speed impulsive noise of a two-bladed rotor which is usually characterized by one large negative pressure peak. BVI noise, however, consists of multiple peaks. The technique works well for waveforms with distinct, repeatable features, but for a four-bladed rotor undergoing weak BVI, selection of an appropriate averaging marker becomes subjective. This difficulty is illustrated in Figs. 8(a) and 8(b) which present an averaged event together with two of the 32 unaveraged events for a weak and strong BVI condition, respectively. The strong BVI condition of Fig. 8(b) is shown for three separate rotor revolutions in Fig. 9. Figures 8 and 9 give an indication of the variability between the same event from revolution to revolution and also the variability between the four events for different revolutions, respectively.

As discussed earlier, the YO-3A is a relatively quiet aircraft. The background noise of the YO-3A is shown compared with the measured helicopter noise for three different flight conditions in Fig. 10. Except for Fig. 10(c) at frequencies greater than 1200 Hz, the background noise level is typically well below the S-76C noise level.

Wind Tunnel Data

The test section of the 80- by 120-Foot Wind Tunnel is acoustically treated, with 6 in absorbent lining on the ceiling and floor and 10 in absorbent lining on the walls.

The sound absorption coefficient is predicted to be at least 0.9 for frequencies greater than 250 Hz. The effect of the wind tunnel floor boundary layer on the acoustic measurements was determined to be unimportant after analyzing data from microphones placed at different heights in the test section. Reflection tests revealed the wind tunnel floor caused reflections with magnitudes about one-half of the single impulsive noise source magnitude. This occasionally caused difficulty in distinguishing between a weak BVI and a reflection. Attempts to minimize the reflections could have been more thoroughly investigated during the test set-up.

Averaged and unaveraged wind tunnel data are shown in Fig. 11. Conditions are similar to the flight conditions of Fig. 8. Figure 11(a) represents a weaker BVI condition than Fig. 11(b). Choosing a repeatable marker for the data of Fig. 11(a) was not possible and so the rotor 1/rev spike was used for averaging. Figure 12 shows the variability between four BVI events for several revolutions of the data for the strong BVI condition of Fig. 11(b). Figure 13 shows the measured rotor noise in the wind tunnel compared with the wind tunnel background noise for the three conditions presented in this paper. The background noise includes the RTA and rotating hub (without blades) in addition to the wind tunnel fan drive noise. The background noise is in general 10 dB lower than the rotor noise for frequencies less than 1000 Hz for Figs. 13(a) and 13(b). Figure 13(c), which is for the highest advance ratio, shows a 10 dB difference only out to approximately 800 Hz.

As discussed earlier, the rotor in the wind tunnel was trimmed by zeroing the 1/rev cyclic flapping angles. In flight, the S-76C pilot trims the rotor propulsive and lift forces while zeroing the helicopter roll and pitching moments. The differences in trim methods will cause slight differences between the tip-path-plane angle in the wind tunnel and in flight.

Results

Table 4 provides a list of flight conditions including overall sound levels in dB_{SL}. Also shown are the wind tunnel conditions which match three of the flight conditions (203, 39_24; 307, 48_19; 315, 48_18). All acoustic flight data presented are from the YO-3A tail microphone. Because of the coarseness of the flight condition matrix, a thorough analysis of parametric effects on BVI noise is not possible. However, some observations are provided on the effects of tip-path-plane angle and advance ratio in the next section, followed by comparisons with wind tunnel data. Although the nondimensional parameters C_T, μ, M_{tip}, and α_{tpp} were matched as closely as possible when comparing flight and wind tunnel data, there are other important effects which are difficult if not impossible to measure or control. A primary example is blade tracking. In the wind tunnel, the blades are only tracked for a few specific conditions at one azimuth; therefore, the term "tip-path plane" refers to an idealized plane through the mean path of all four blades. Although the wind tunnel and flight blades are not perfectly tracked for all conditions and azimuths, when analyzing blade-to-blade differences in the data, effects of tracking are assumed small.

Parametric Effects

Figure 14 shows the effect of increasing tip-path-plane angle while holding the other important nondimensional parameters (C_T, μ, M_{tip}) nearly constant. The effect is similar to that shown for a full-scale and a corresponding small-scale two-bladed rotor in Ref. 4. As the tip-path plane is tilted further back, achieved by increasing descent rate, the likelihood of the blades intersecting with older vortices becomes more probable, since the rotor wake begins to move upward through the rotor. As explained in Ref. 4, the older vortices will be intersected by the blade at smaller azimuth angles (earlier in time). This phenomenon can be manifested in the waveforms by the appearance of peaks reaching a maximum earlier in time, as shown by the arrows in Fig. 14. Note that the initial positive peak preceding the larger group of three peaks increases with magnitude as α_{tpp} is increased so that finally in Fig. 14(c) , there are four distinct BVIs per blade. This effect is also shown in Fig. 15 to a much lesser degree. In Fig. 15(b), the small growth of a positive peak preceding the group of four larger peaks is noticed for each blade.

Figure 16 shows the effect of increasing μ, achieved by increasing forward speed and descent rate simultaneously in order to maintain a nearly constant α_{tpp}. Figure 16(a) reveals some secondary BVI not evident in Fig. 16(b). A possible explanation is that the rotor wake geometry is not as stable at the lower advance ratio compared to the higher advance ratio case, causing more inconsistent BVI. The blade-to-blade differences in Fig. 16(a) are much more noticeable than in Fig. 16(b). Also, the magnitude of the BVI is increased by 2.3 dB_{SL} at the higher advance ratio (compare flight points 308 and 315 in Table 4).

Comparisons with Wind Tunnel Data

Following the practice of previous studies, the flight and wind tunnel data are compared in the time domain. Three matching conditions are presented in Figs. 17, 18, and 19 corresponding to low, moderate, and high advance ratio cases, respectively.

Figures 17(a) and 17(b) compare averaged waveforms for a low speed, strong BVI case for one revolution and

one-quarter revolution, respectively. Because of the slight differences in rotor rpm during the flight and wind tunnel tests, the two waveforms have been aligned a quarter revolution at a time. The similarity in the peak widths and magnitude are quite good, although the peaks in the flight data appear greater in magnitude generally. The noise level measured in flight is slightly (1.2 dB_{SL}) higher than the level measured in the wind tunnel (compare flight point 203 and wind tunnel point 39_24 in Table 4). The flight data show three to four vortex interactions per blade. The wind tunnel data also show this; however, multiple lower level pulses are also clearly evident. There are several negative peaks prior to the major BVI and several positive peaks following the major BVI. This pattern is repeated for all four blades in the wind tunnel. Analysis of the reflection test data indicate that some of the low level pulses following the major BVI may be due to floor reflections, while the smaller pulses preceding the major BVI may be caused by ceiling reflections and/or weak primary vortex interactions.

The pulse width is an indication of the core size of the vortex filament interacting with the blade. Figure 17(b) reveals that the pulse widths of the flight and wind tunnel data are very similar. This is not surprising since two similar full-scale rotors are being compared and the viscous effects should be directly comparable. Reproducing full-scale viscous effects using small-scale models is always a concern because of Reynolds number effects. The similarity in pulse widths also indicates that the tip-path-plane angle in the wind tunnel and in flight were similar despite the difference in trim methods.

The frequency content of the flight and wind tunnel time histories shown in Fig. 17(a) are presented in Figs. 10(a) and 13(a), respectively. The flight data show the characteristic BVI feature (energy spikes at blade passage harmonics inside a scalloped envelope) for the entire frequency range shown. The wind tunnel spectrum envelope is not as clean, possibly due to reflections The flight noise levels are generally higher for frequencies greater than 600 Hz compared with the wind tunnel noise levels.

A moderate advance ratio condition is shown in Fig. 18. Compared to Fig. 17, this condition is for a much lower thrust coefficient. Major peak widths match well, although magnitudes differ by as much as 5 Pa or more. Table 4 shows that the flight noise level is 2.3 dB_{SL} lower than the wind tunnel level (compare flight point 307 and wind tunnel point 48_19). The flight data also show evidence of high-speed impulsive noise represented by the wider, negative peak following the three to four BVIs for each blade. The wind tunnel data again display the lower level impulses adjacent to the major BVI, although the impulses are not as prominent compared to Fig. 17. The frequency spectra of the flight and wind tunnel data are shown in Figs. 10(b) and 13(b), respectively. Figures 10(b) and 13(b) are much more similar than the spectra pair of Figs. 10(a) and 13(a).

Figure 19 represents the highest advance ratio condition of the three matched cases. Conditions are similar to Fig. 18 except for advance ratio. The noise level in flight is 1.2 dB_{SL} lower than the wind tunnel level (compare flight point 315 and wind tunnel point 48_18 in Table 4). Although the two waveforms are presented overlayed, no attempt was made to align the two waveforms in time since the shapes are so different. Also, averaging the wind tunnel data using the technique described earlier was impossible due to blade-to-blade and revolution-to-revolution differences in the data. Instead, the wind tunnel data were averaged using the rotor 1/rev signal. Differences in averaging methods are possibly contributing to the poor comparison shown in Fig. 19.

Figures 20 and 21 present the waveforms for each one-quarter revolution of the wind tunnel and flight test data, respectively, shown in Fig. 19. Similar features exist in each quarter of a revolution of the wind tunnel data in Fig. 20, but appear highly distorted from one blade to another. Figure 21, however, shows that the blades in flight experience similar interactions with the rotor wake. For this condition, the 80- by 120-Foot Wind Tunnel environment is not an adequate substitute for the free-air environment. Interestingly, Ref. 6 observed a deterioration in the scalability of BVI noise at high advance ratios ($\mu > 0.22$). The frequency spectra of the flight and wind tunnel data of Fig. 19 are shown in Figs. 10(c) and 13(c), respectively. For this condition, the signal-to-noise ratio in flight and in the wind tunnel is worse compared to the lower speed cases, hence contributing to the poor comparison shown in Fig. 19.

Conclusions

In-flight acoustic measurements of an S-76C helicopter were acquired using the NASA Ames YO-3A research aircraft. Within the context of the limited flight test matrix, parametric effects on BVI noise are discussed. Comparisons with full-scale wind tunnel data are also shown. Specific findings include:

1. For the conditions presented, increasing tip-path-plane angle causes the appearance of BVI peaks reaching a maximum earlier in time; these observations are similar to those observed in two-bladed rotor flight test data and small-scale data.

2. Increasing advance ratio increases the magnitude of the BVI noise for the conditions presented.

3. For the low and moderate advance ratio conditions presented, the BVI pulse widths of the flight and wind tunnel data are very similar.

4. Noise levels measured in the wind tunnel are within 2.5 dB_{SL} of the levels measured in flight.

5. The small impulses immediately preceding and following major BVI in the wind tunnel data do not appear in the flight data and may be caused by reflections.

6. Comparisons between the flight and wind tunnel data waveforms for the high advance ratio case ($\mu \approx 0.25$) are poor. For this condition, the wind tunnel data show greater blade-to-blade and revolution-to-revolution variability than the flight data.

Acknowledgements

The authors thank Dr. Marianne Mosher and Dr. Fred Schmitz of NASA Ames Research Center for their valuable advice regarding the analysis of the data. The contributions of Mr. Martin Hagen and Mr. Cahit Kitaplioglu of NASA Ames Research Center are acknowledged for their work in the acquisition of S-76 rotor acoustic data in the 80- by 120-Foot Wind Tunnel. The efforts of many people from NASA Ames and Sikorsky Aircraft contributed to this successful flight test program. In particular, the efforts of the following people are greatly appreciated: Dan Hoang, NASA Ames, YO-3A Instrumentation Engineer; Munro Dearing, NASA Ames, YO-3A Pilot; George Tucker, NASA Ames, S-76C Co-Pilot; Tom Davis, Sikorsky Aircraft, S-76C Pilot.

References

1. Schmitz, F. H. and Boxwell, D. A., "In-Flight Far-Field Measurement of Helicopter Impulsive Noise," American Helicopter Society 32nd Annual Forum, Washington, D. C., May 1976.

2. Vause, C. R., Schmitz, F. H., and Boxwell, D. A., "High-Speed Helicopter Impulsive Noise," American Helicopter Society 32nd Annual Forum, Washington, D. C., May 1976.

3. Boxwell, D. A. and Schmitz, F. H., "Full-Scale Measurements of Blade-Vortex Interaction Noise," American Helicopter Society 36th Annual Forum, Washington, D. C., May 1980.

4. Schmitz, F. H., Boxwell, D. A., Lewy, S., and Dahan, C., "Model-to Full-Scale Comparisons of Helicopter Blade-Vortex Interaction Noise," *Journal of the American Helicopter Society*, Vol. 29, (2), Apr. 1984.

5. Splettstoesser, W. R., Schultz, K. J., Schmitz, F. H., and Boxwell, D. A., "Model Rotor High-Speed Impulsive Noise- Parametric Variations and Full-Scale Comparisons," American Helicopter Society 39th Annual Forum, St. Louis, Missouri, May 1983.

6. Splettstoesser, W. R., Schultz, K. J., Boxwell, D. A., and Schmitz, F. H., "Helicopter Model Rotor-Blade Vortex Interaction Impulsive Noise: Scalability and Parametric Variations," Tenth European Rotorcraft Forum, The Hague, The Netherlands, Aug. 1984.

7. Splettstoesser, W. R., Schultz, K. J., and Martin, R. M., "Rotor Blade-Vortex Interaction Impulsive Noise Source Identification and Correlation with Rotor Wake Predictions," AIAA-87-2744, AIAA 11th Aeroacoustics Conference, Palo Alto, California, Oct. 1987.

8. Martin, R. M., Splettstoesser, W. R., Elliot, J. W., and Schultz, K. J., "Advancing-Side Directivity and Retreating-Side Interactions of Model Rotor Blade-Vortex Interaction Noise," NASA TP 2784, AVSCOM TR 87-B-3, May 1988.

9. Burley, C. L. and Martin, R. M., "Tip-Path-Plane Angle Effects on Rotor Blade-Vortex Interaction Noise Levels and Directivity," American Helicopter Society 44th Annual Forum, Washington, D. C., Jun. 1988.

10. Martin, R. M., Marcolini, M. A., Splettstoesser, W. R., and Schultz, K. J., "Wake Geometry Effects on Rotor Blade-Vortex Interaction Noise Directivity," NASA TP 3015, Aug. 1990.

11. Marcolini, M. A., Martin, R. M., Lorber, P. F., and Egolf, T. A., "Prediction of BVI Noise Patterns and Correlation with Wake Interaction Locations," American Helicopter Society 48th Annual Forum, Washington, D. C., Jun. 1992.

12. Cross, J. L. and Watts, M. E.,"Tip Aerodynamics and Acoustics Test," NASA RP 1179, Dec. 1988.

13. Cross, J. L., "YO-3A Acoustics Research Aircraft Systems Manual," NASA TM 85968, Jul. 1984.

14. Cross, J. L. and Watts, M. E., "In-Flight Acoustic Testing Techniques Using the YO-3A Acoustic Research Aircraft," NASA TM 85895, Feb. 1984.

15. Watts, M. E., "ALDAS User's Manual," NASA TM 102381, Apr. 1991.

Table 1. S-76C Aircraft Characteristics

Aircraft Tail No.	N3123U
Empty weight with fuel	9797 lb
Fuel capacity	1850 lb
Max. cruise speed @ sea level	approximately 150 kts
Equivalent flat plate area	12.6 ft^2
Longitudinal c.g.	station 210 inches
Lateral c.g.	station 0.0 inches

Table 2. S-76C Rotor Characteristics

Main rotor	
Number of blades	4
Rotor radius	22 ft
Nominal chord	15.5 in
Solidity ratio	0.0748
Flapping hinge offset	3.79% radius
Lock number	11.6
Airfoils	SC1013-R8, SC1095-R8, SC1095
Normal operating rpm	313 (100% = 293 rpm)
Tail rotor	
Number of blades	4
Normal operating rpm	1723 (@ 313 main rotor rpm)

Table 3. YO-3A Aircraft Characteristics

Wingspan	57 ft
Length	29.3 ft
Height	9.1 ft
Maximum gross takeoff weight	3800 lb
Propeller diameter	100 in
Stall speed	60 kts (approx. IAS)
Maximum speed	110 kts (approx. IAS)
Power plant	210 hp (Continental)
Aircraft type	single engine, tail dragger
Number of propeller blades	3
Propeller tip speed	360 ft/s

Table 4. Flight and wind tunnel test conditions.

Test point	V_D (ft/min)	M_{tip}	V_{true} (kts)	μ	C_T	p_o/p_{SLo}	α_{tpp}[2] (deg)	α_{tpp}[3] (deg)	dB_{SL}
Flight									
203[a]	748	0.603	65.8	0.164	0.00778	0.7857	6.3	5.6	106.2
205	970	0.609	74.7	0.183	0.00694	0.8545	6.0	6.2	98.8
208	585	0.614	100	0.244	0.00675	0.8512	0.5	1.2	109.6
209	870	0.607	100	0.246	0.00682	0.8557	1.8	2.8	105.4
213	181	0.613	67.1	0.164	0.00678	0.8320	0.8	0.6	100.0
304	843	0.615	68.4	0.167	0.00670	0.8199	5.6	6.0	101.2
305	863	0.611	66.8	0.164	0.00667	0.8293	5.7	6.4	102.7
306	272	0.605	80.0	0.196	0.00608	0.9244	-0.3	0.4	99.9
307[b]	306	0.606	82.7	0.203	0.00605	0.9227	0.1	0.5	100.3
308	250	0.606	76.9	0.189	0.00600	0.9272	0.2	0.4	101.4
309	438	0.608	82.5	0.202	0.00601	0.9152	0.8	1.4	103.1
312	868	0.604	78.4	0.193	0.00608	0.9050	4.3	4.8	101.2
315[c]	490	0.606	100	0.245	0.00600	0.9017	-0.4	0.4	103.7
Wind tunnel									
39_24[a]	741	0.605	69.0	0.173	0.00753	1.0045	5.0[1]		105.0
48_17	473	0.604	100	0.251	0.00598	1.0041	0.0[1]		104.9
48_18[c]	475	0.605	100	0.251	0.00597	1.0041	0.0[1]		104.9
48_19[b]	245	0.605	79.9	0.200	0.00599	1.0041	0.0[1]		102.6

[1] shaft angle
[2] from Eq. (2)
[3] from Eq. (3)

[a, b, c] matching conditions

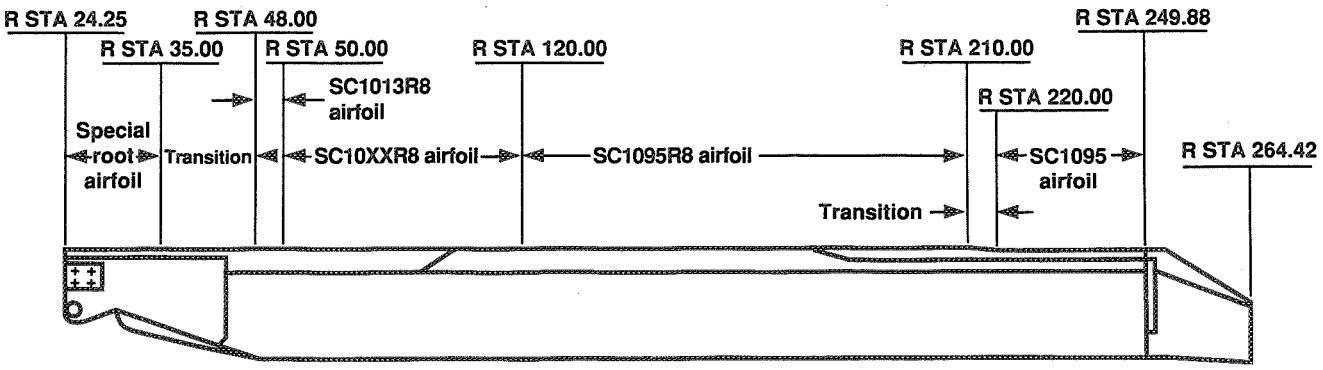

Figure 1. S-76C rotor blade features.

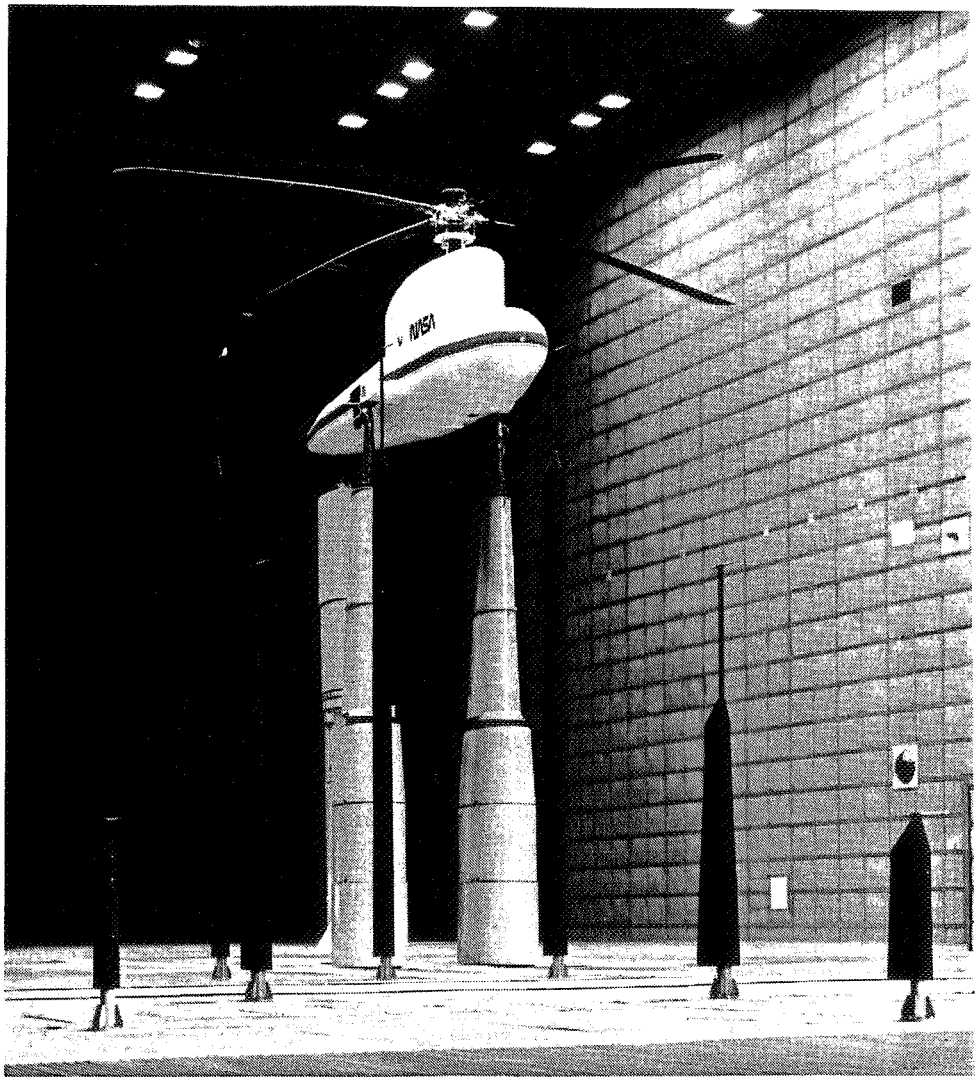

Figure 2. S-76 rotor installation in the 80- by 120-Foot Wind Tunnel.

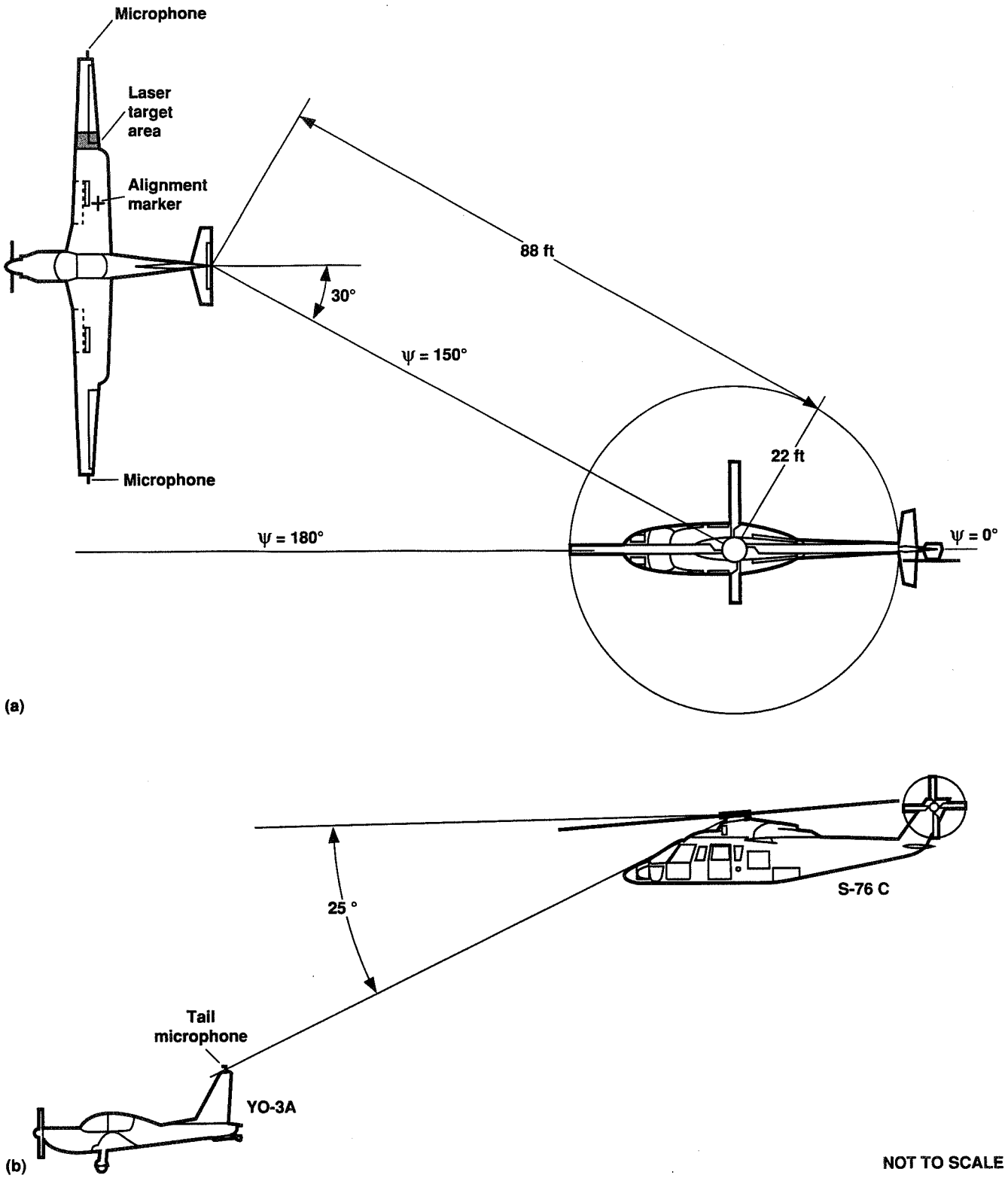

Figure 3. Flight formation (a) plan view (b) side view

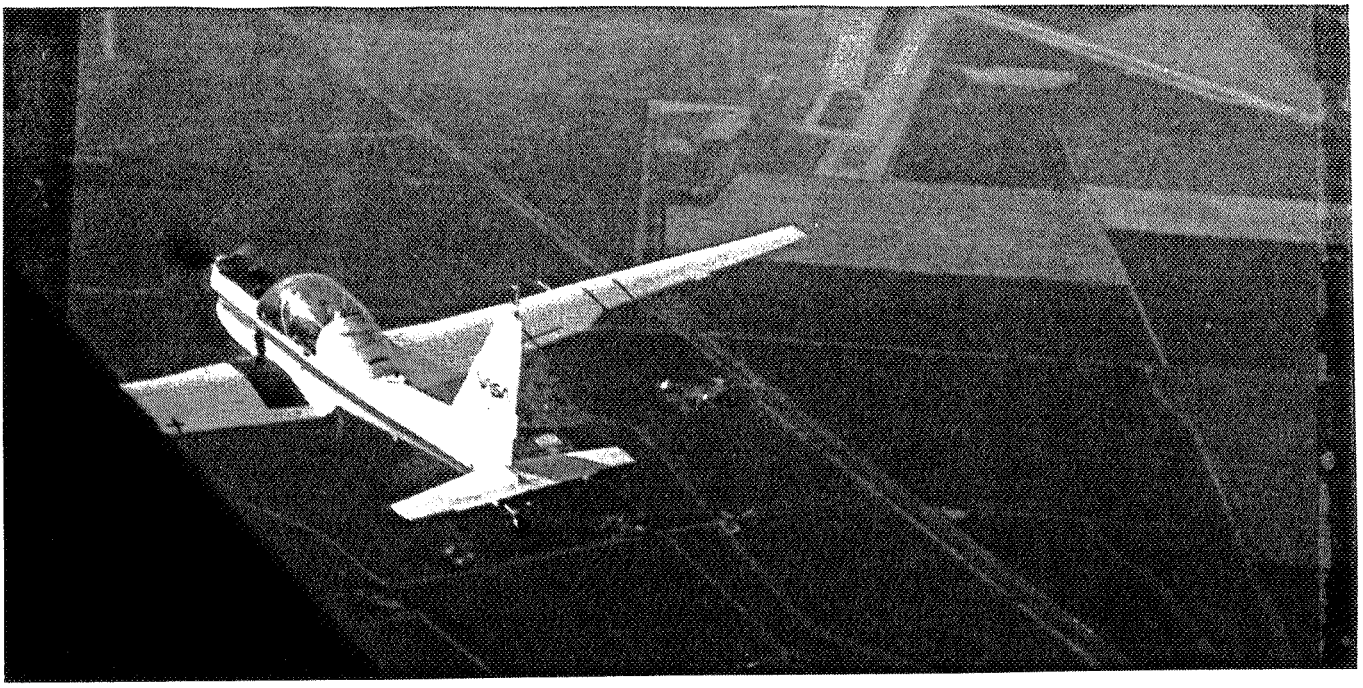

Figure 4. Formation view from helicopter passenger compartment.

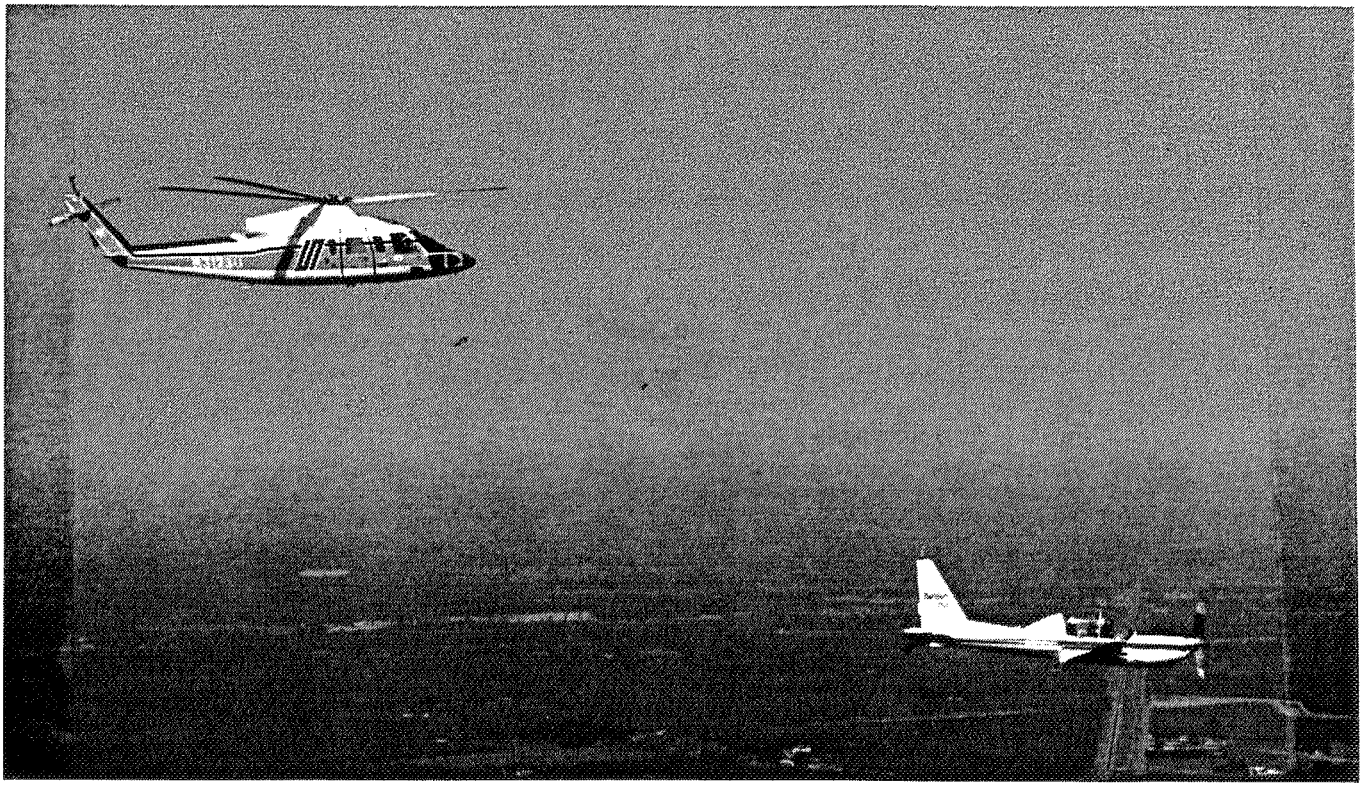

Figure 5. Formation side view.

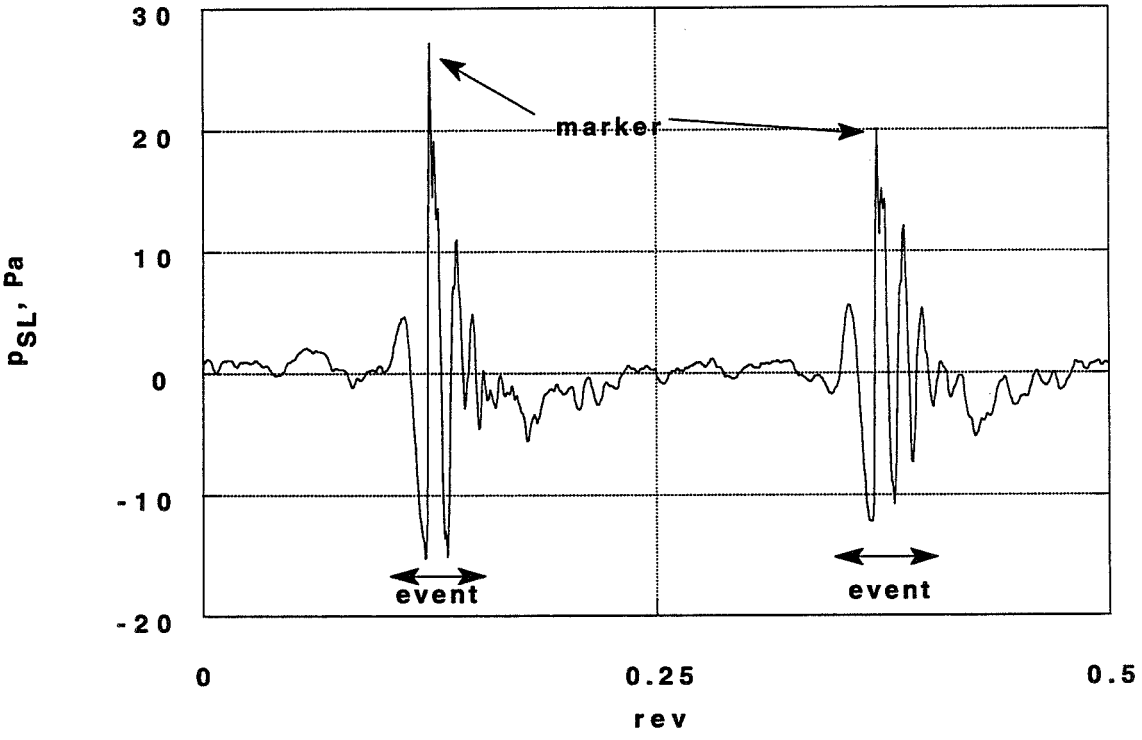

Figure 6. BVI time history features.

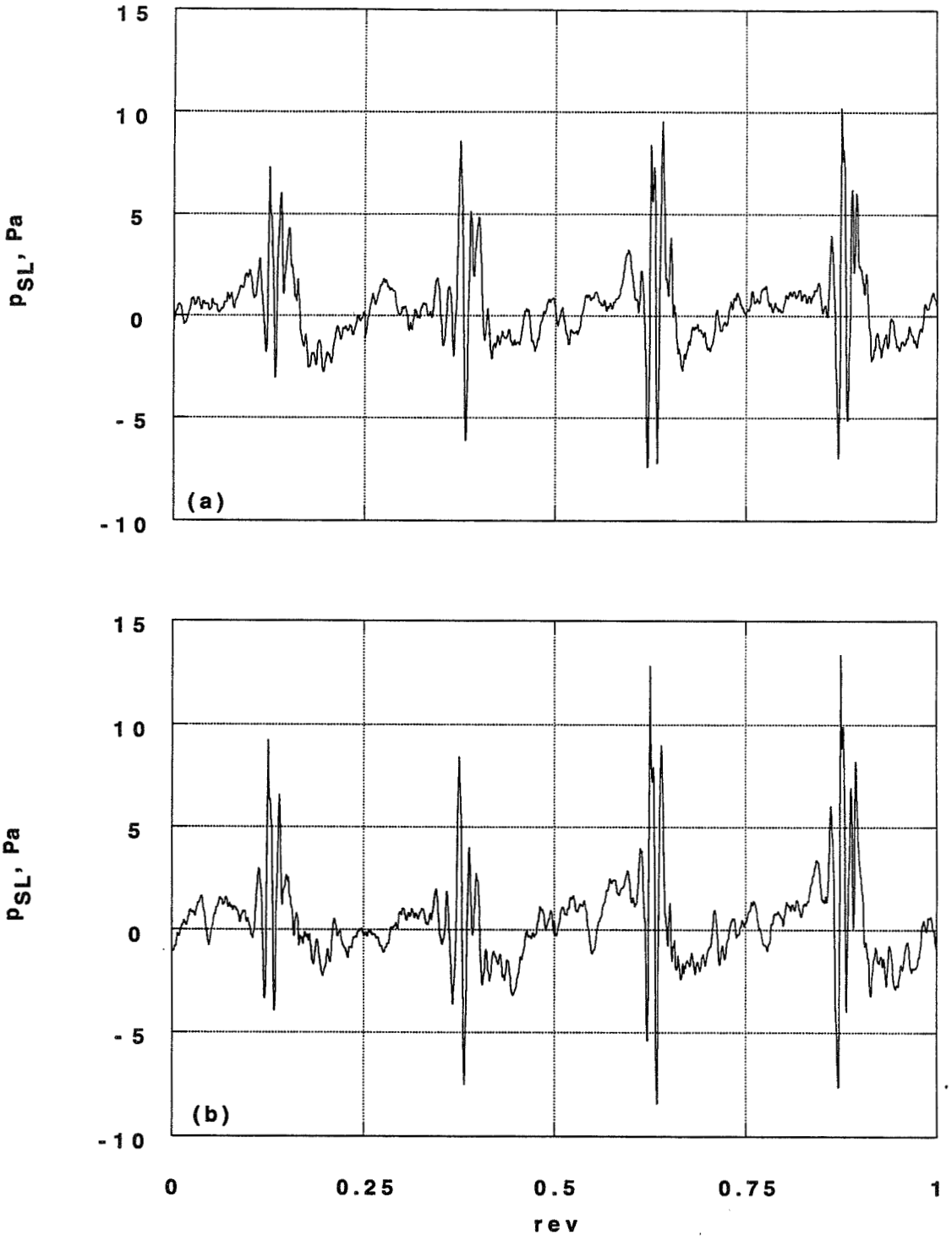

Figure 7. Repeatability of flight test data. (a) Flight pt. 304 conditions: C_T=0.00670, M_{tip}=0.615, α_{tpp}=6.0 deg, μ=0.167 (b) Flight pt. 305 conditions: C_T=0.00667, M_{tip}=0.611, α_{tpp}=6.4 deg, μ=0.164

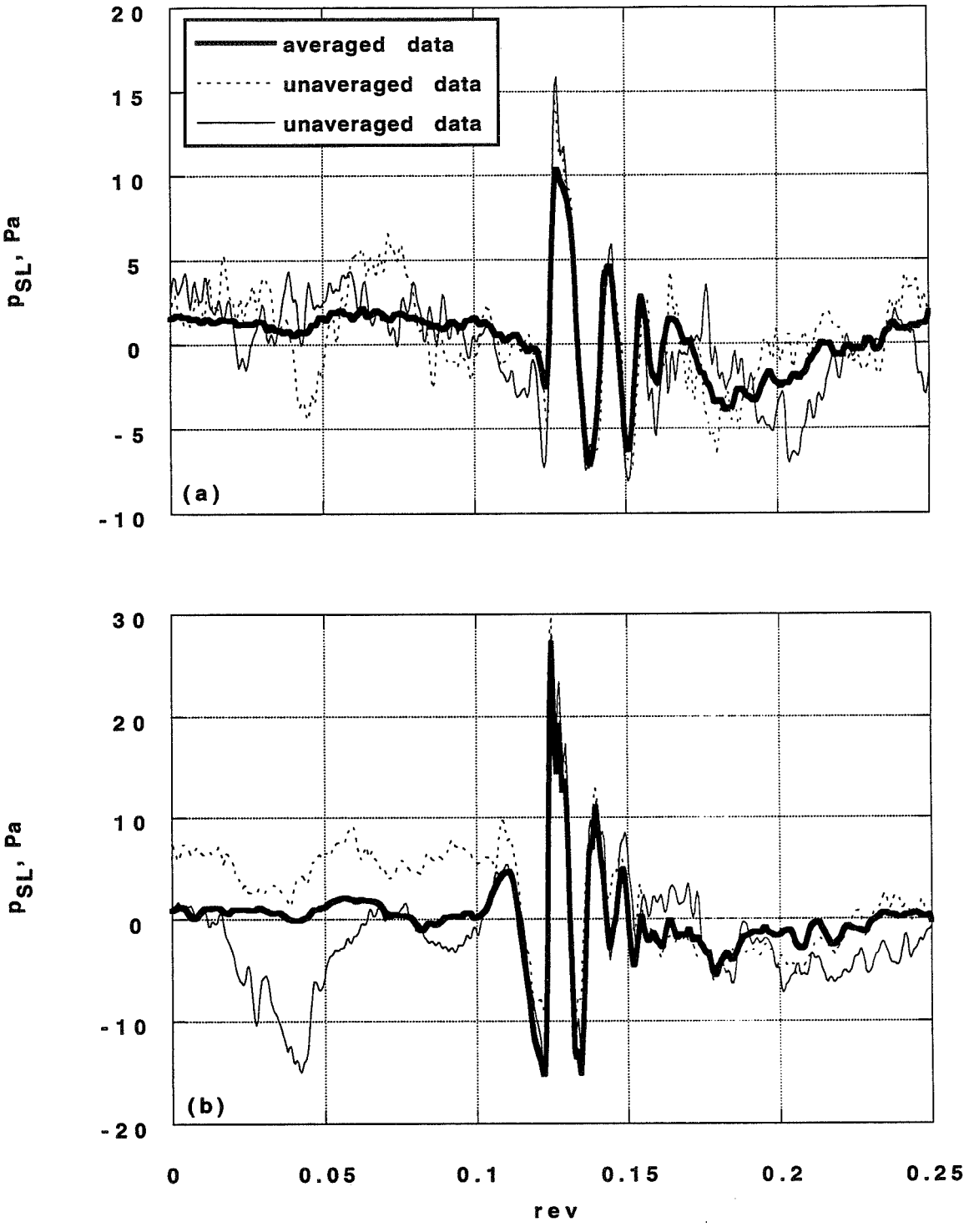

Figure 8. Averaged and unaveraged data. (a) Flight pt. 315 conditions: C_T=0.00600, M_{tip}=0.606, μ=0.245, α_{tpp}=0.4 deg (b) Flight pt. 203 conditions: C_T=0.00778, M_{tip}=0.603, μ=0.164, α_{tpp}=5.6 deg

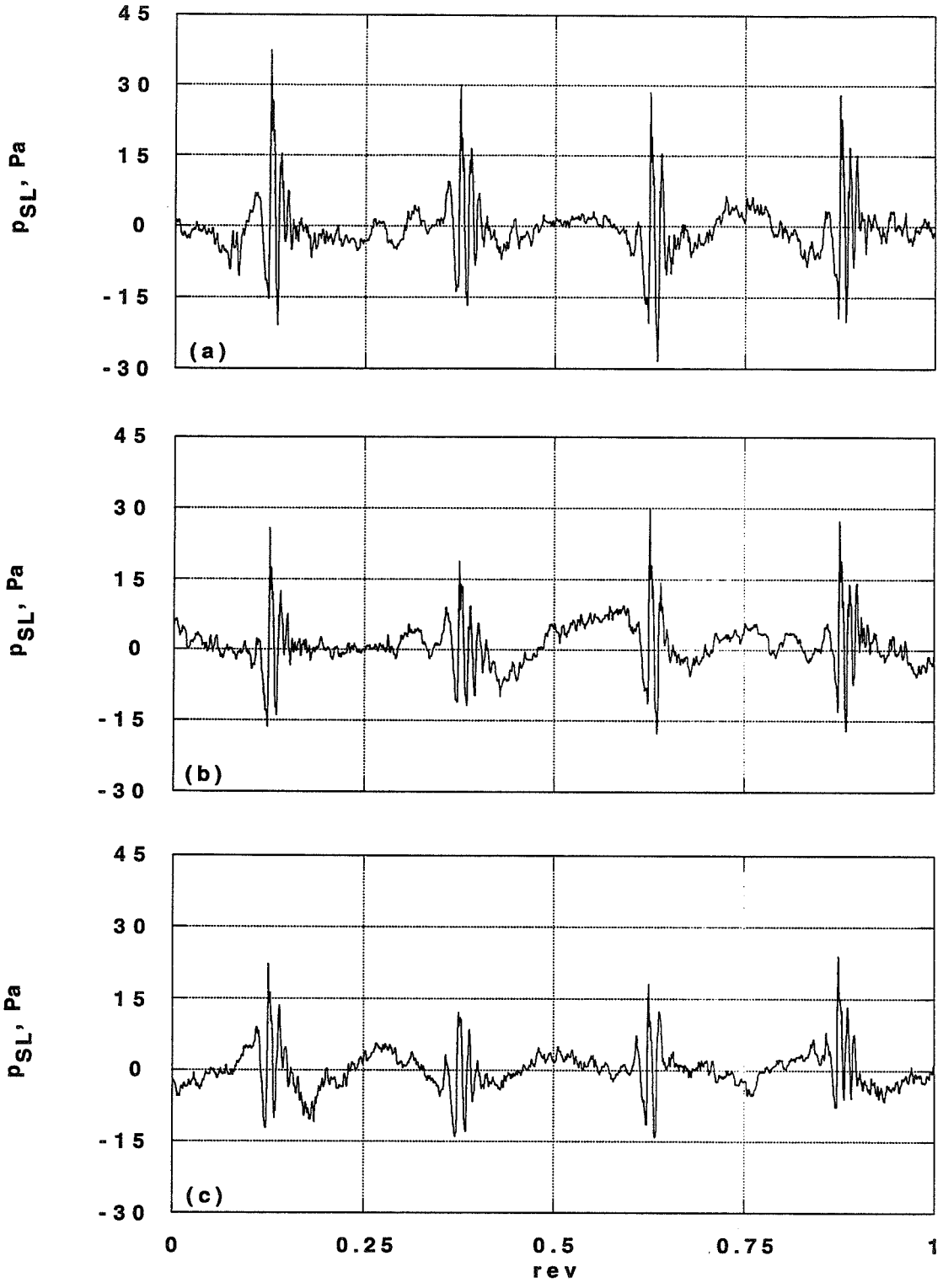

Figure 9. Variability in unaveraged data. Flight pt. 203 conditions: C_T=0.00778, M_{tip}=0.603, μ=0.164, α_{tpp}=5.6 deg. (a) rev 1 (b) rev 4 (c) rev 20

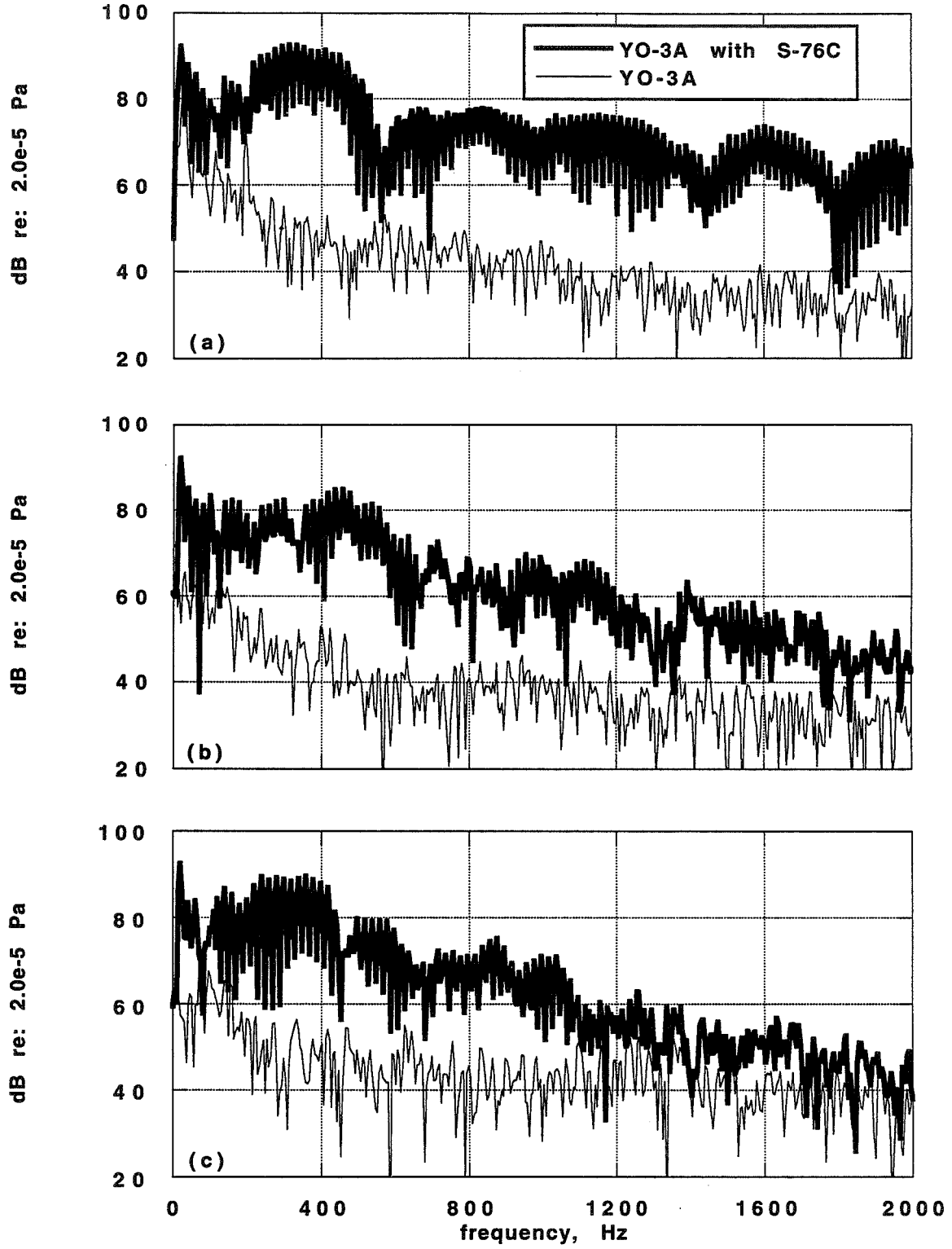

Figure 10. YO-3A background noise. (a) Flight pt. 203 conditions: C_T=0.00778, M_{tip}=0.603, μ=0.164 (b) Flight pt. 307 conditions: C_T=0.00605, M_{tip}=0.606, μ=0.203 (c) Flight pt. 315 conditions: C_T=0.00600, M_{tip}=0.606, μ=0.245

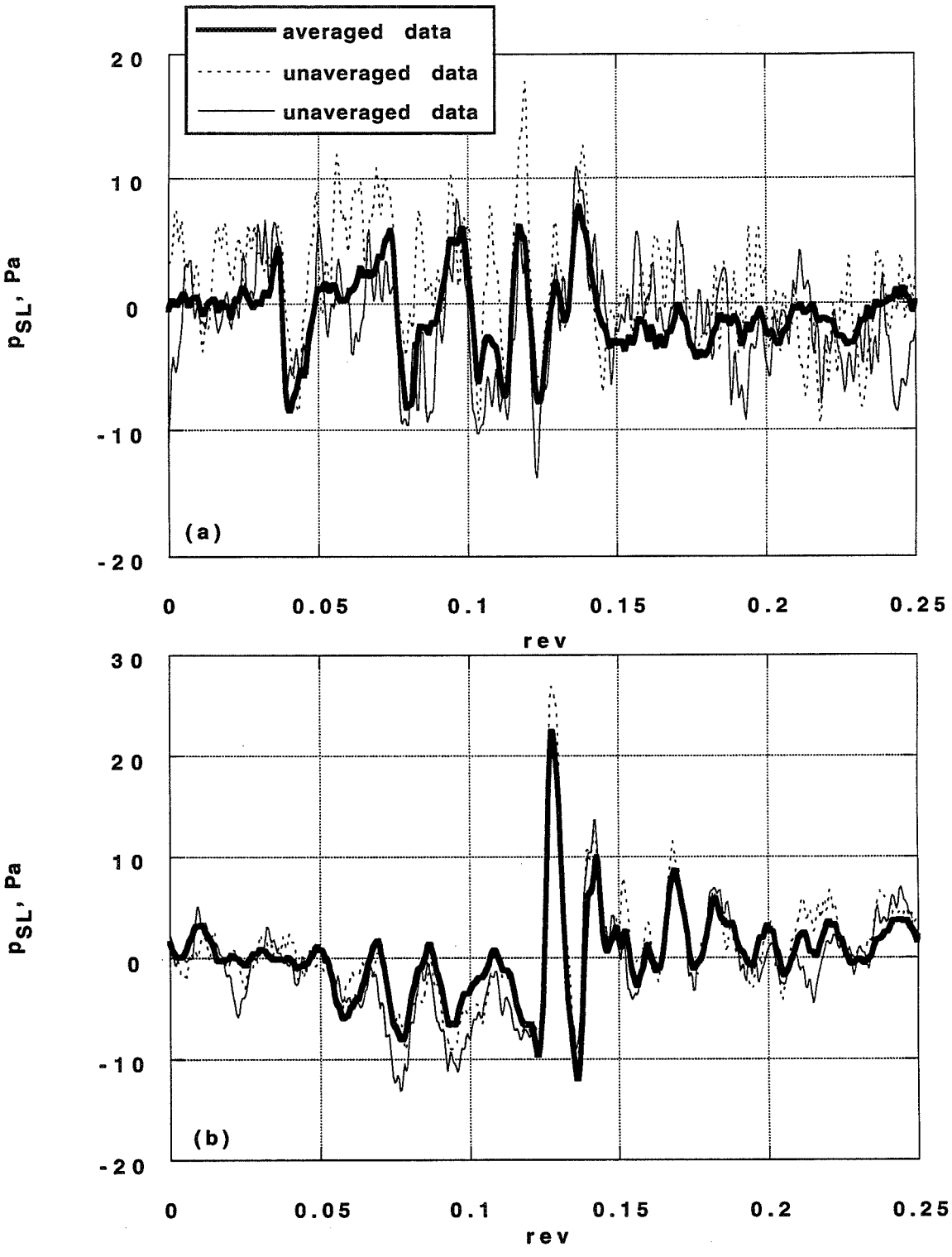

Figure 11. Averaged and unaveraged data. (a) Wind tunnel pt. 48_18 conditions: C_T=0.00597, M_{tip}=0.605, μ=0.251, α_{tpp}=0.0 deg (b) Wind tunnel pt. 39_24 conditions: C_T=0.00753, M_{tip}=0.605, μ=0.173, α_{tpp}=5.0 deg

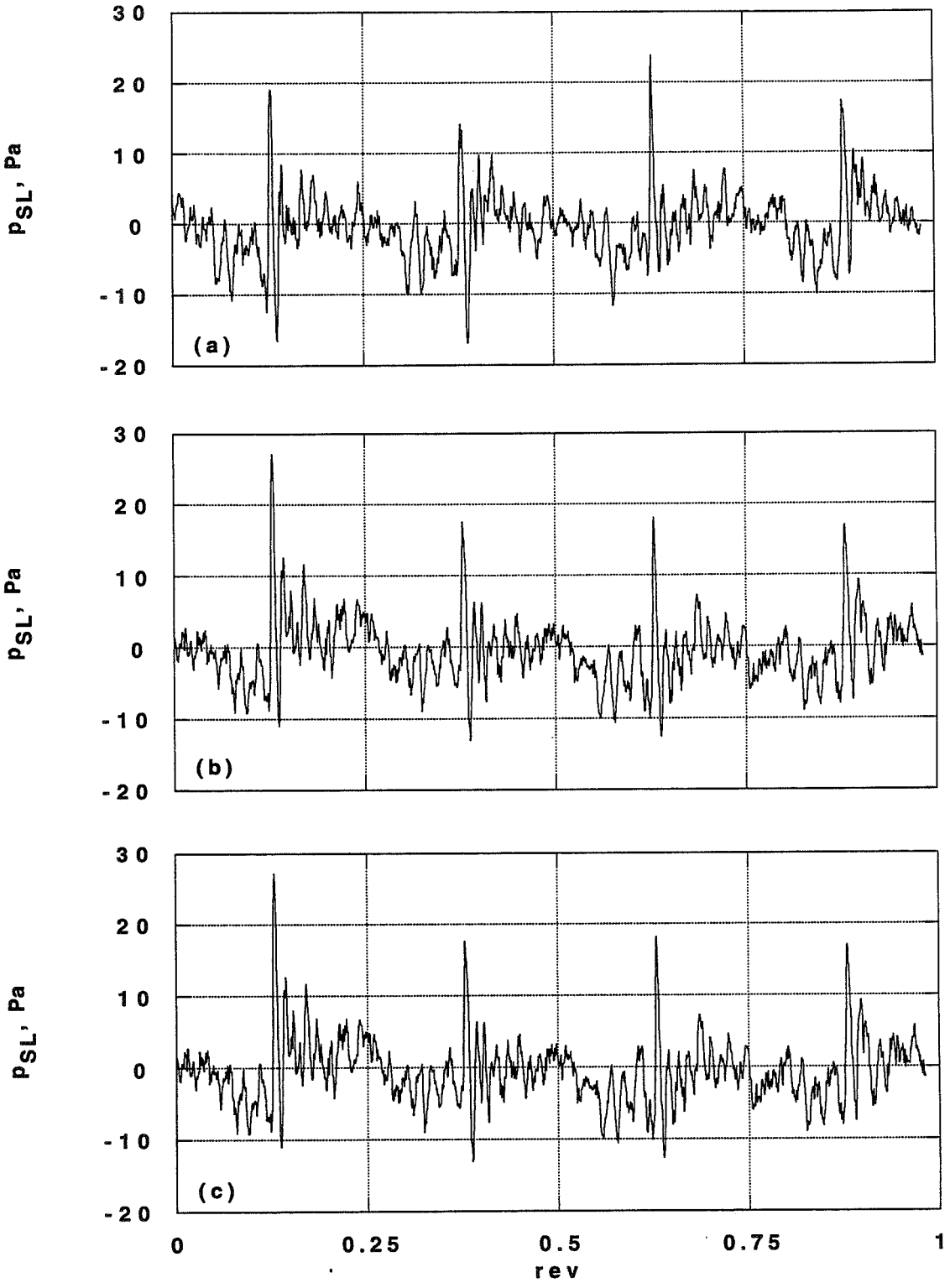

Figure 12. Variability in unaveraged data. Wind tunnel pt. 39_24 conditions: C_T=0.00753, M_{tip}=0.605, μ=0.173, α_{tpp}=5.0 deg (a) rev 1 (b) rev 15 (c) rev 30

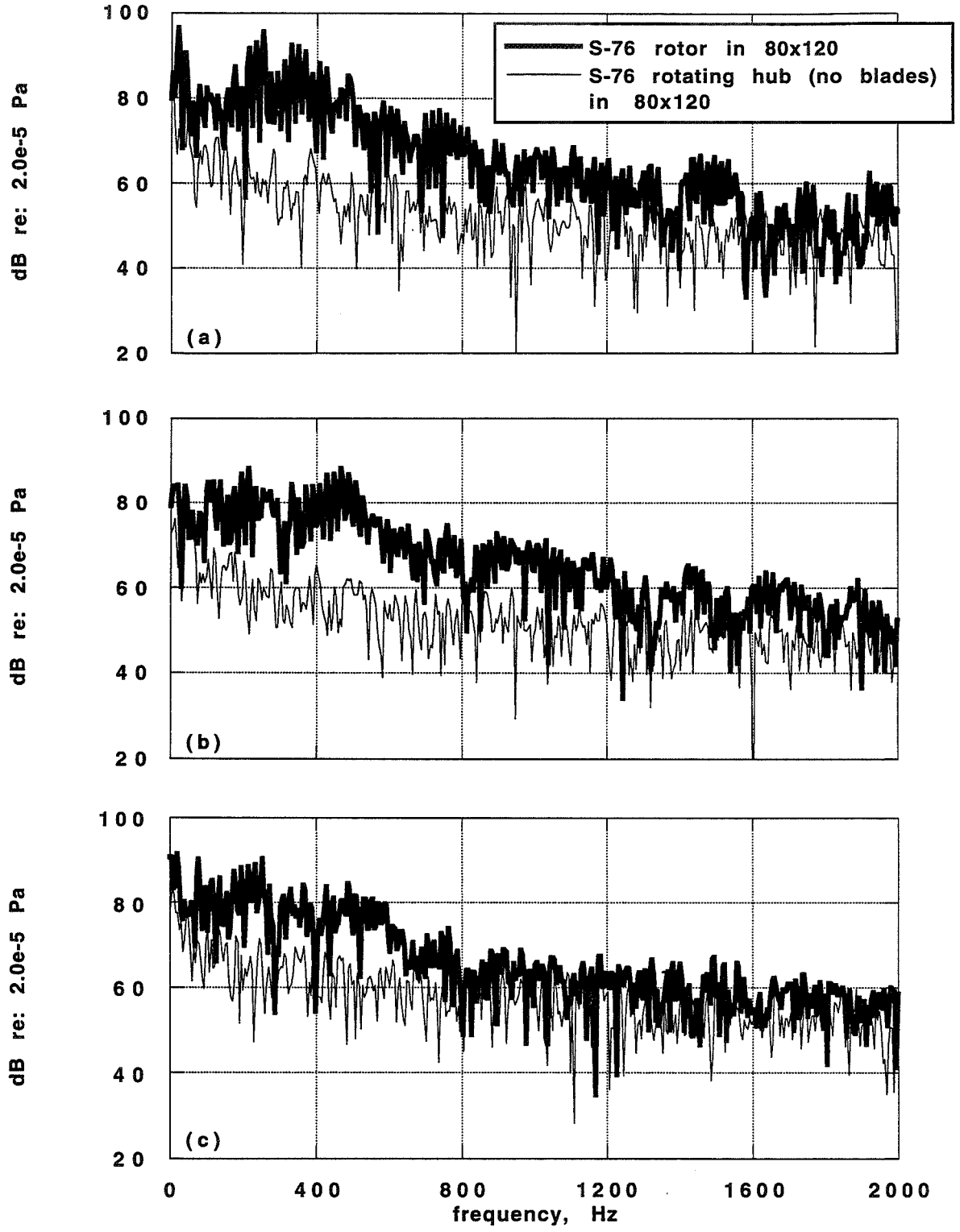

Figure 13. Wind tunnel background noise. (a) Run 39_24 conditions: C_T=0.00753, M_{tip}=0.605, μ=0.173, α_{tpp}=5.0 deg (b) Run 48_19 conditions: C_T=0.00599, M_{tip}=0.605, μ=0.200, α_{tpp}=0.0 deg (c) Run 48_18 conditions: C_T=0.00597, M_{tip}=0.605, μ=0.251, α_{tpp}=0.0 deg.

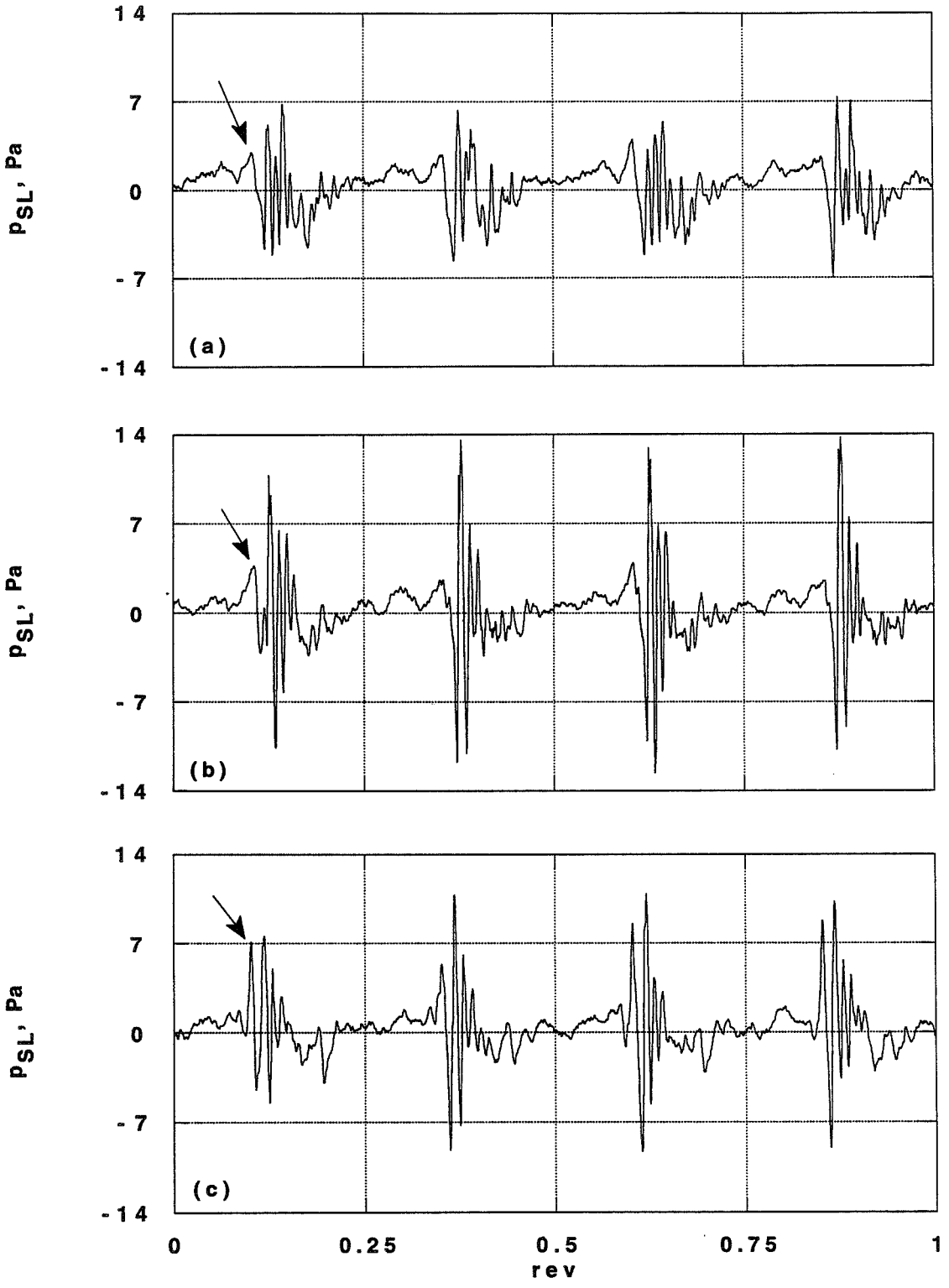

Figure 14. Effect of α_{tpp}. (a) Flight pt. 306 conditions: C_T=0.00608, M_{tip}=0.605, μ=0.196, α_{tpp}=0.4 deg (b) Flight pt. 309 conditions: C_T=0.00601, M_{tip}=0.608, μ=0.202, α_{tpp}=1.4 deg (c) Flight pt. 312 conditions: C_T=0.00608, M_{tip}=0.604, μ=0.193, α_{tpp}=4.8 deg

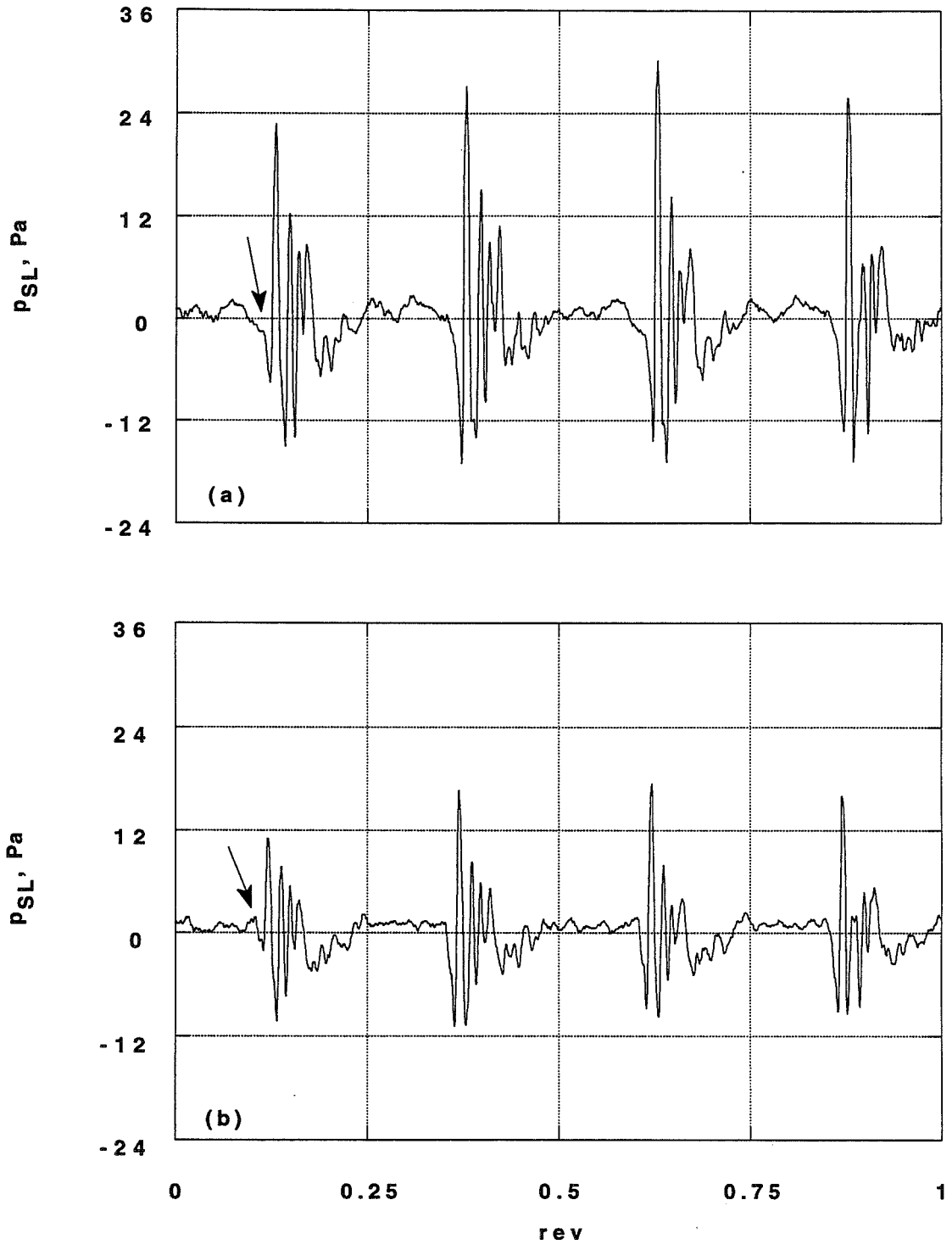

Figure 15. Effect of α_{tpp}. (a) Flight pt. 208 conditions: C_T=0.00675, M_{tip}=0.614, μ=0.244, α_{tpp}=1.2 deg (b) Flight pt. 209 conditions: C_T=0.00682, M_{tip}=0.607, μ=0.246, α_{tpp}=2.8 deg

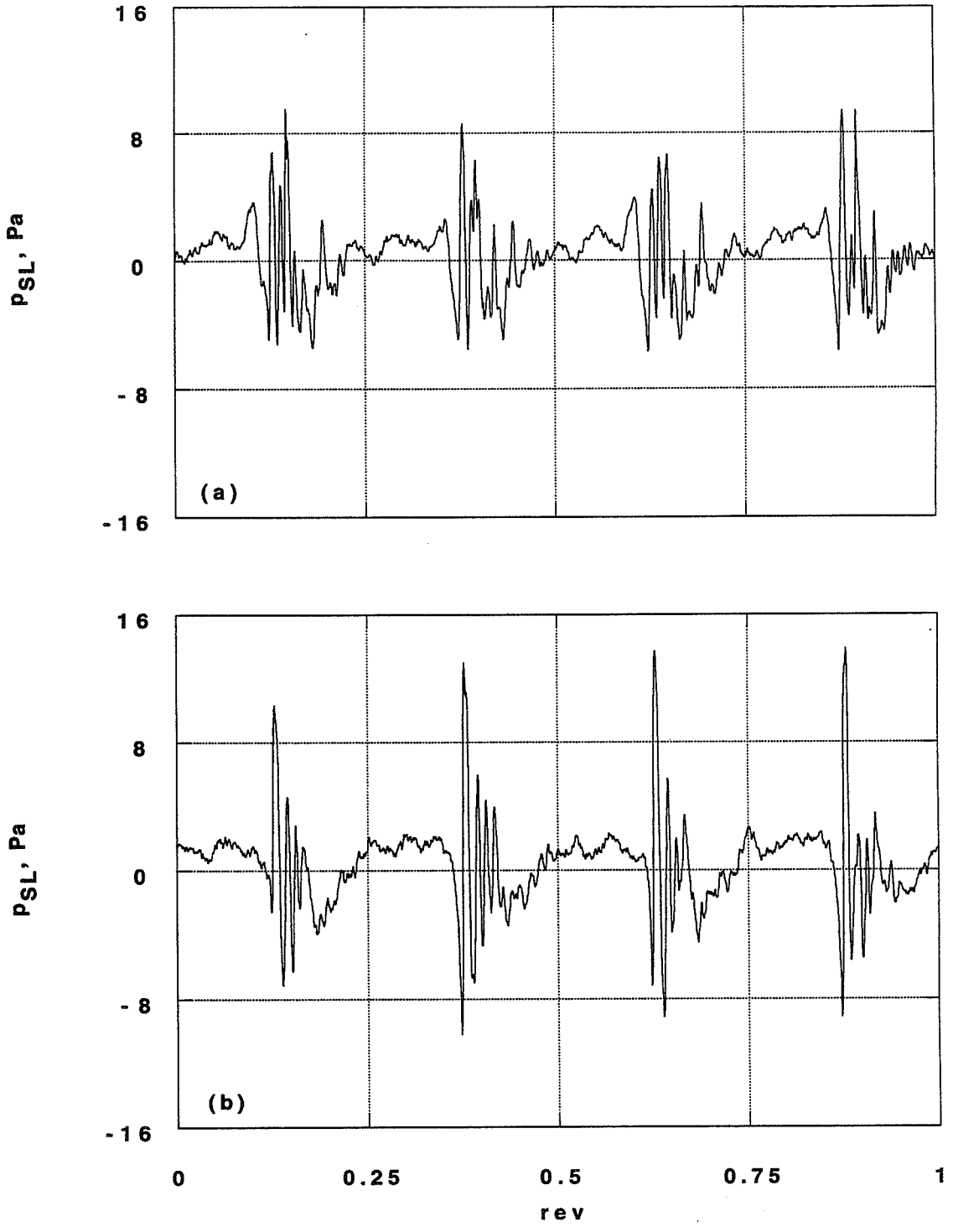

Figure 16. Effect of advance ratio. (a) Flight pt. 308 conditions: C_T=0.00600, M_{tip}=0.606, α_{tpp}=0.4 deg, μ=0.189 (b) Flight pt. 315 conditions: C_T=0.00600, M_{tip}=0.606, α_{tpp}=0.4 deg, μ=0.245

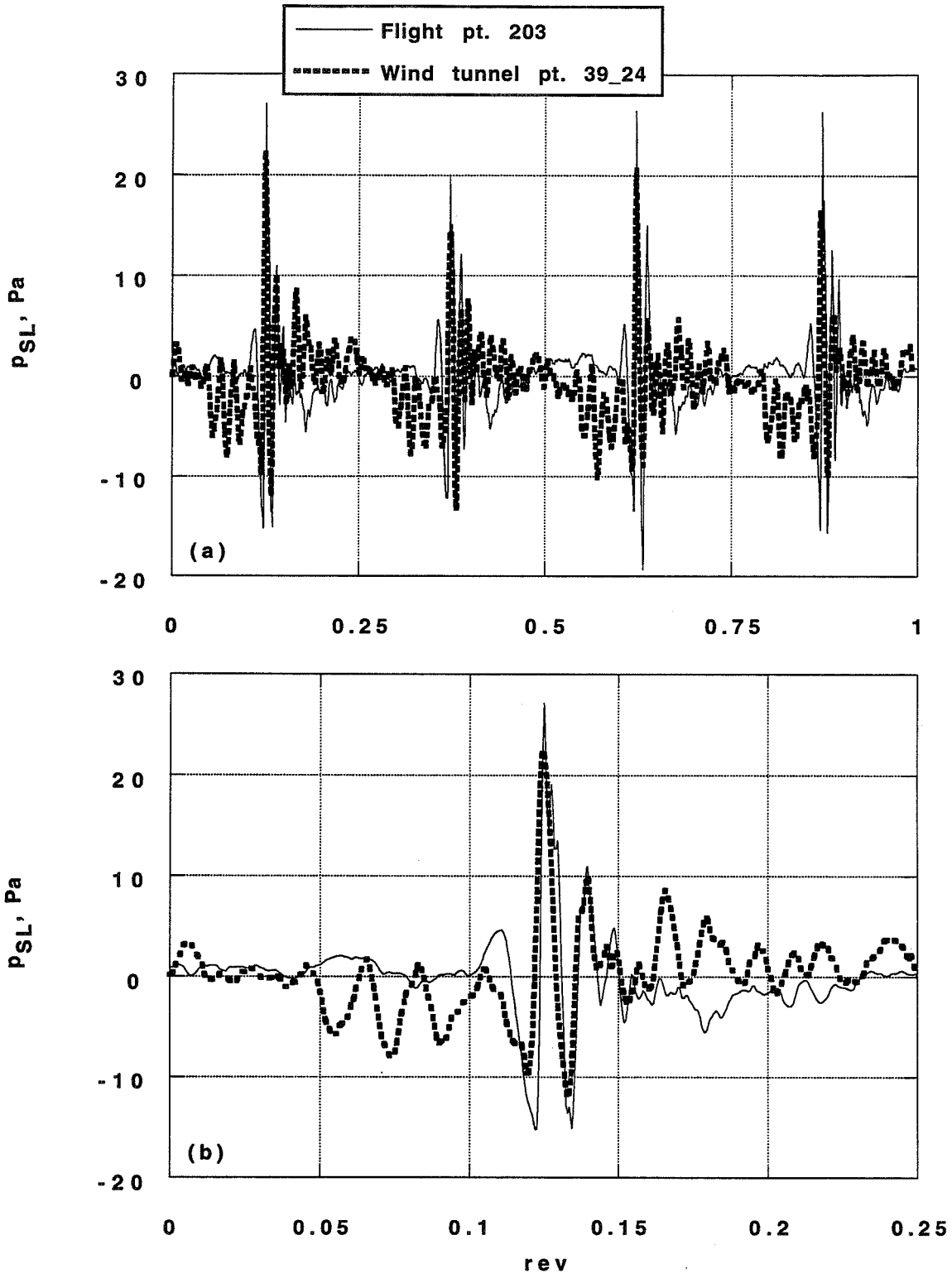

Figure 17. Flight and wind tunnel data comparison. Flight pt. 203 conditions: C_T=0.00778, M_{tip}=0.603, μ=0.164, α_{tpp}=5.6 deg. Run 39_24 conditions: C_T=0.00753, M_{tip}=0.605, μ=0.173, α_{tpp}=5.0 deg. (a) one revolution (b) 1/4 revolution

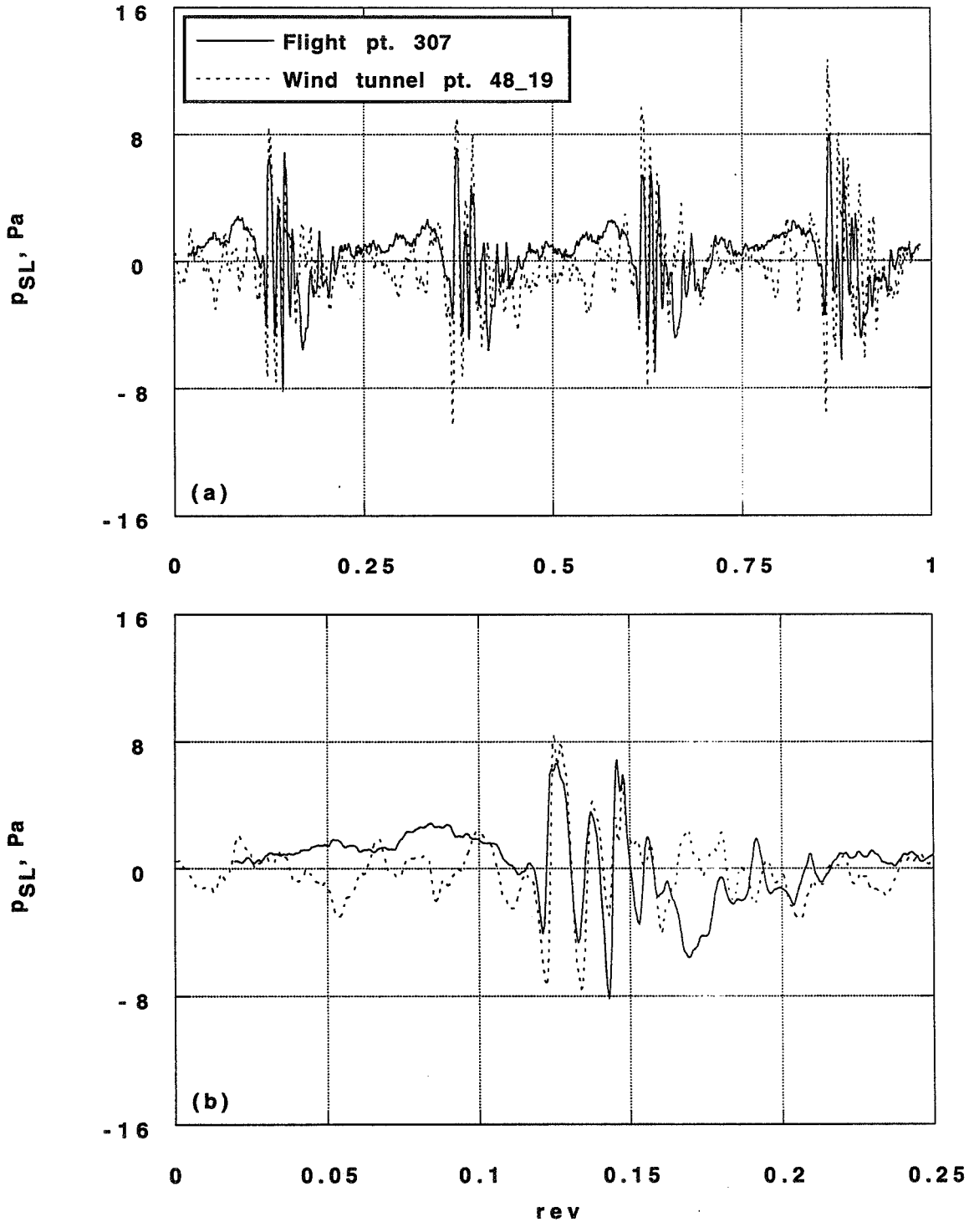

Figure 18. Flight and wind tunnel data comparison. Flight pt. 307 conditions: C_T=0.00605, M_{tip}=0.606, μ=0.203, α_{tpp}=0.5 deg. Run 48_19 conditions: C_T=0.00599, M_{tip}=0.605, μ=0.200, α_{tpp}=0.0 deg. (a) one revolution (b) 1/4 revolution

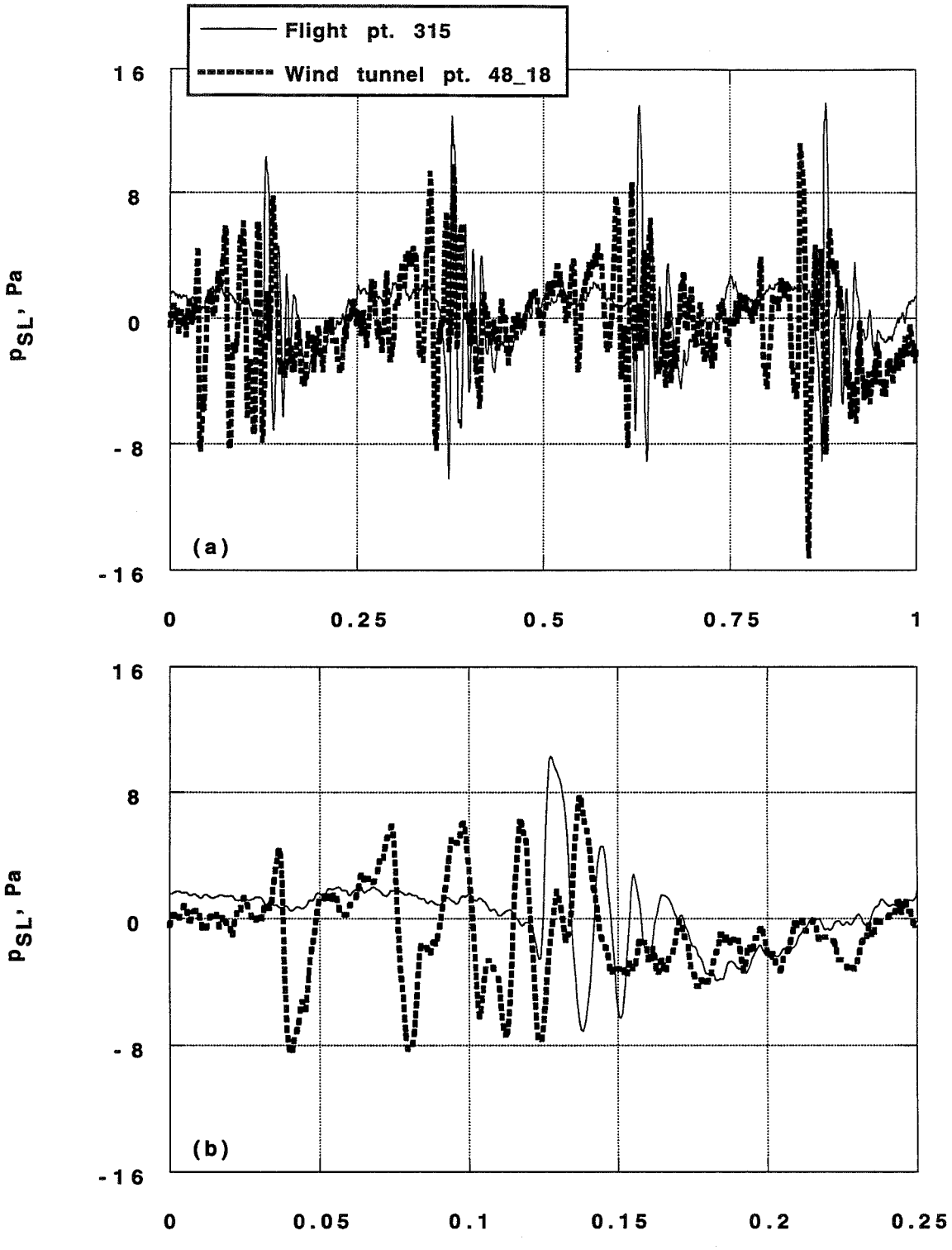

Figure 19. Flight and wind tunnel data comparison. Flight pt. 315 conditions: C_T=0.00600, M_{tip}=0.606, μ=0.245, α_{tpp}=0.4 deg. Run 48_18 conditions: C_T=0.00597, M_{tip}=0.605, μ=0.251, α_{tpp}=0.0 deg. (a) one revolution (b) 1/4 revolution

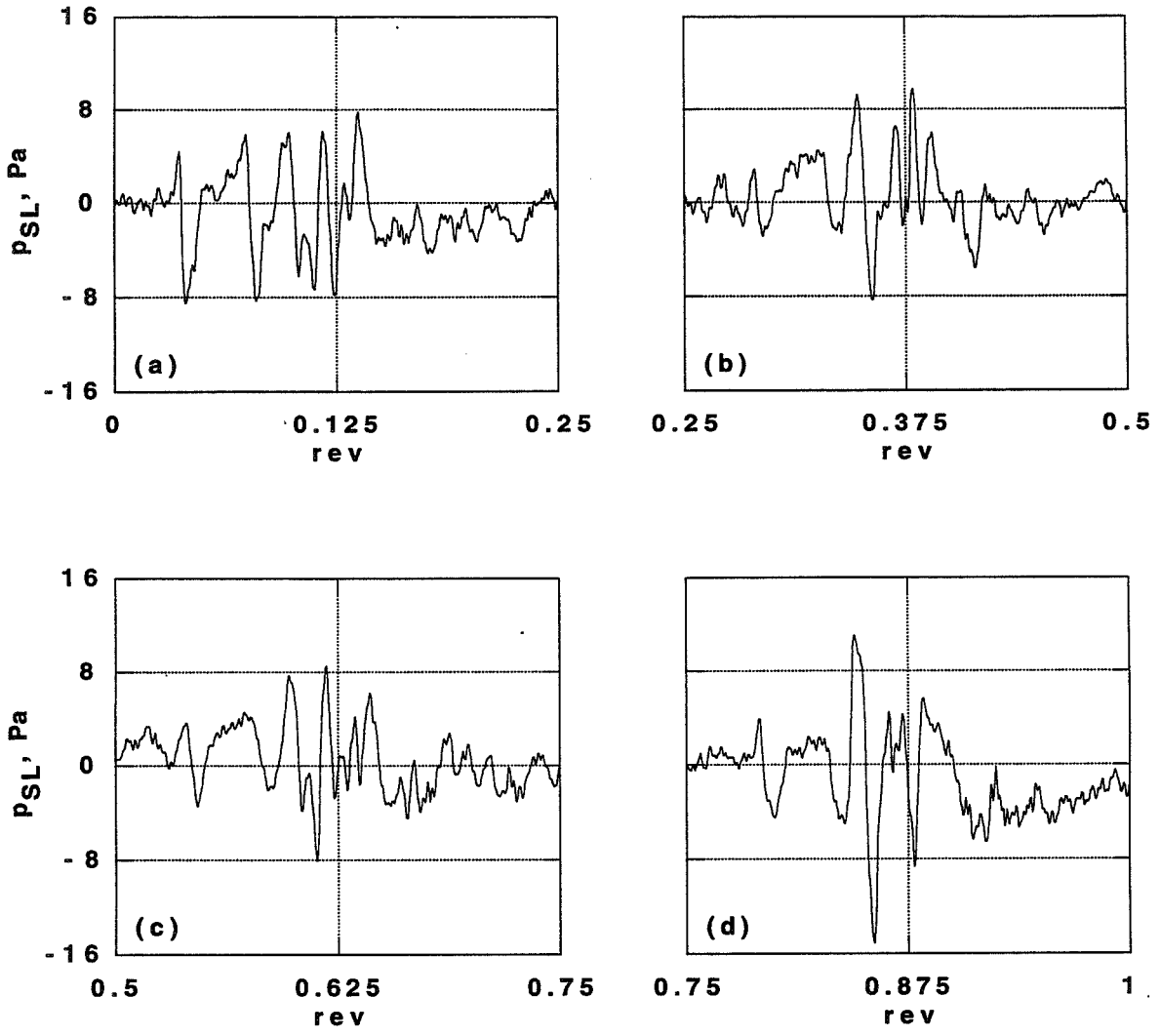

Figure 20. Blade-to-blade variability of wind tunnel data. Run 48_18 conditions: C_T=0.00597, M_{tip}=0.605, μ=0.251, α_{tpp}=0.0 deg. (a) blade1 (b) blade 2 (c) blade 3 (d) blade 4

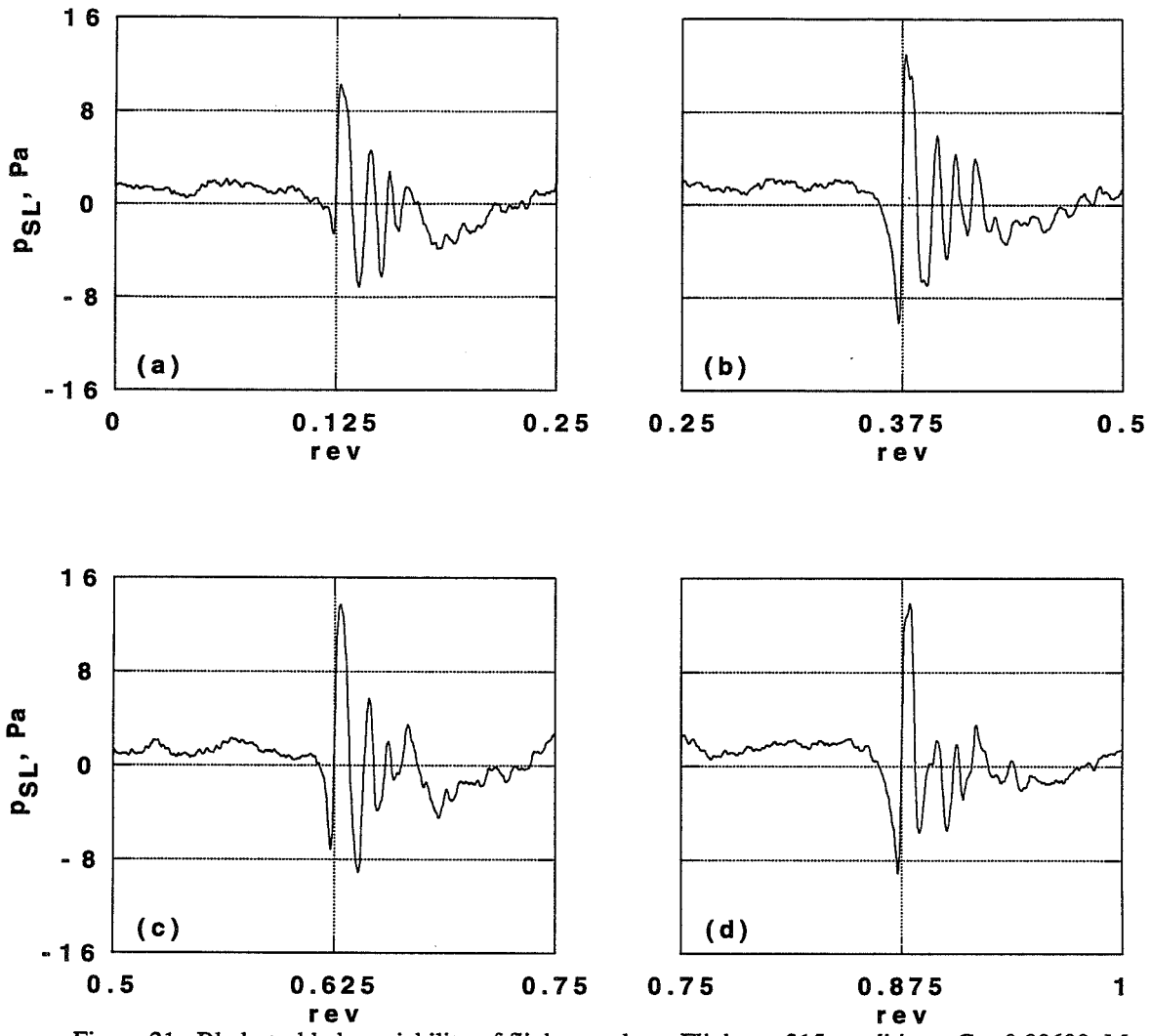

Figure 21. Blade-to-blade variability of flight test data. Flight pt. 315 conditions: C_T=0.00600, M_{tip}=0.606, μ=0.245, α_{tpp}=0.4 deg. (a) blade1 (b) blade 2 (c) blade 3 (d) blade 4